Food Hydrocolloids 154 (2024) 110127

Contents lists available at ScienceDirect

Food Hydrocolloids

journal homepage: www.elsevier.com/locate/foodhyd

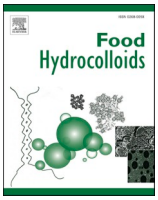

Fibrillisation of faba bean protein isolate by thermosonication for process efficacy: Microstructural characteristics, assembly behaviour, and physicochemical properties

Yinxuan Hu [a], Lirong Cheng [b], Elliot Paul Gilbert [c,d], Trevor S. Loo [e], Sung Je Lee [a], John Harrison [f], Zhi Yang [a,*]

[a] School of Food and Advanced Technology, Massey University, Auckland, 0632, New Zealand
[b] Riddet Institute, Massey University, Palmerston North, 4472, New Zealand
[c] Australian Centre for Neutron Scattering, ANSTO, New Illawarra Road, Lucas Heights, NSW, 2234, Australia
[d] Australian Institute for Bioengineering and Nanotechnology and Centre for Nutrition and Food Sciences, The University of Queensland, St. Lucia, Brisbane, QLD, Australia
[e] BioProtection Aotearoa, School of Natural Sciences, Massey University, Palmerston North, 4410, New Zealand
[f] School of Natural Sciences, Massey University, Auckland, 0632, New Zealand

ARTICLE INFO

Keywords:
Thermosonication
Self-assembly fibrils
Faba bean protein isolates
Small angle neutron scattering
High internal phase emulsions
Microstructures

ABSTRACT

The effect of thermosonication (TS) (90 °C, 10–30 min) on the fibrillisation of faba bean protein isolate (FPI) was studied. The self-assembly behaviour, microstructural characteristics and techno-functional (gelation and emulsification) properties of FPI fibrils obtained from TS treatment were compared with those obtained from conventional prolonged heating (CH) at 90 °C up to 8 h. Compared to CH treatment, TS treatment was shown to significantly accelerate the formation of FPI fibrils with prominent β-sheet structures as revealed by Thioflavin T (ThT) fluorescence, Fourier-transform infrared spectroscopy (FTIR) and circular dichroism (CD). The characteristics of fibril building blocks were analysed by sodium dodecyl sulfate-polyacrylamide gel electrophoresis (SDS-PAGE) and liquid chromatography linked to tandem mass spectrometry (LC-MS/MS) to obtain the differences between TS and CH induced fibrillisation of FPI. Transmission electron microscopy (TEM) and small-angle neutron scattering (SANS) showed that 4 h CH and 10 min TS treatments resulted in the fibrils with similar radius (from 5 to 10 nm). Furthermore, SANS indicated that TS treatment induced the formation of an entangled FPI fibrillar network, which could lead to the observed viscoelastic properties of FPI at a high concentration (10 wt %). Finally, high internal phase O/W emulsions (HIPE, $\varphi = 0.75$) stabilised by 30 min TS induced FPI fibrils (3 wt %) demonstrated a stronger gel strength and smaller oil droplet size compared to those prepared with untreated FPI, suggesting a superior emulsification capability of FPI fibrils. This finding demonstrates that TS treatment is a promising and efficient method for fibrillisation of plant proteins with the resultant fibrils generating excellent gelation and emulsification properties.

1. Introduction

Proteins form a variety of ordered or disordered structures including fibrils, branched structures, flexible strands, or random aggregates after denaturation (Bolder et al., 2006). Among these structures, amyloid-like fibrils enriched in β-sheets have attracted extensive attentions due to their unique structural and physicochemical properties (Meng et al., 2022; Ye et al., 2019). Due to their high aspect ratio with exposure of functional groups exposed on the surface upon fibrillisation, protein fibrils demonstrate enhanced gelation behaviour (Chen et al., 2020), improved emulsification capacity (Gao, et al., 2017), and superior mechanical properties (Xu, et al., 2022) compared to native proteins. Therefore, fibrillisation has been regarded as an efficient and promising method for improving protein techno-functionalities (Meng, et al., 2022).

To date, fibrillisation has been achieved for a wide range of food proteins, including whey protein isolate (Yang, Jiao, et al., 2022), egg white proteins (Alavi, Emam-Djomeh, Mohammadian, Salami, &

* Corresponding author.
E-mail address: Z.Yang2@massey.ac.nz (Z. Yang).

https://doi.org/10.1016/j.foodhyd.2024.110127
Received 26 October 2023; Received in revised form 19 April 2024; Accepted 22 April 2024
Available online 22 April 2024

Moosavi-Movahedi, 2020), soybean protein isolate (Wang, et al., 2020), and hemp protein concentrate (Kutzli, Zhou, Li, Baier, & Mezzenga, 2023). Recently, fibrillisation of plant proteins has been increasingly studied in order to improve their inferior functional properties such as low solubility and poor emulsification capability (Nasrabadi, Doost, & Mezzenga, 2021). Until now, the commonly used method to induce food protein fibrillisation is a prolonged heat treatment (i.e. 12-96 h) at high temperatures (e.g. 80–90 °C) and pH 2, which are energy-intensive and time-consuming. In addition, sample pretreatments including centrifugation, membrane filtration, and/or pre-solubilisation of proteins in strong denaturants such as guanidine chloride (GuHCl) have been used in previous studies of fibril formations from plant proteins from different sources including mung bean, lupin, oat, rapeseed proteins (Herneke, et al., 2021), legume proteins (Li, Wang, Zhang, et al., 2021), rice glutelin (Li, Wang, Geng, Zhang, & Chen, 2021), and potato proteins (Josefsson, et al., 2019). These pretreatments were generally conducted to unfold the compact structures of plant proteins and overcome their low water solubility, thereby improving the fibrillisation efficiency and conversion rate (Liu, Yang, Wang, Jiang, & Chen, 2023). However, most treatments are cumbersome, and some may potentially leave residual chemicals in the formed protein fibrils. Therefore, in recent years, various novel and emerging physical treatment strategies such as microwave heating (Zhang, et al., 2020), hydrothermal treatment at high pressure (Yang, Jiao, et al., 2022), and radio frequency heating (Wang, et al., 2023) have been explored in the formation of protein fibrils.

As a green and emerging food processing technology, ultrasonication (US) has been extensively used to modify plant proteins from cereals and legumes (e.g. quinoa and faba bean proteins) (Luo, Yang, Wang, Ashokkumar, & Hemar, 2022; Rahman, Hojilla-Evangelista, & Lamsal, 2022; Wen et al., 2019). The high shear forces, micro-jetting, and shockwaves generated by the US cavitation can disrupt large protein aggregates and improve the solubility of plant proteins (Gharibzahedi & Smith, 2020). However, most previous studies on the US treatment of plant proteins were conducted at a low temperature (e.g. ice-water bath) to prevent protein denaturation. Besides being used as a pretreatment method, US can be directly used for the formation of protein fibrils from recombinant hisactophilin (Stathopulos, et al., 2004), myoglobin (Stathopulos, et al., 2004), and β_2-microglobulin (Ohhashi, Kihara, Naiki, & Goto, 2005). It has been suggested that the strong agitation and the destabilisation of proteins at the air-liquid interface of the cavities formed during US could accelerate spontaneous nucleation of monomeric protein thus promoting the formation of protein fibrils (Ohhashi, et al., 2005; Stathopulos et al., 2004; Yagi, Hasegawa, Yoshimura, & Goto, 2013). However, studies on the formation of food (plant) protein fibrils using US treatment are still very limited. Recently, Kamada et al. (2021) employed US combined with heat treatment (referred to thermosonication (TS)) (70 W, 40% amplitude, 90 °C, 30 min) to treat 10 wt % soybean protein isolate (SPI) in 30% v/v acetic acid solution and found that the SPI fibrils self-assembly occurred after cooling. The film forming capability of SPI fibrils was subsequently studied for packaging applications. They believed that the acetic acid solvent is essential for SPI fibril formation, due to its enhanced solvation of hydrophobic amino acid residues under aqueous-compatible conditions (Kamada, et al., 2021; Mason et al., 2014). This study indicated that TS treatment under specific solvent conditions has the potential to induce fibrillisation of plant proteins. However, the systematic comparison of TS and conventional heat (CH) treatments on the formation of plant protein fibrils and its influence on technofunctional properties (e.g. gelation and emulsification), which are important for their application, have not been reported. Despite there are some recent studies on plant protein fibrils, most of them used prolonged conventional heating to induce fibrillisation (Herneke, et al., 2021; Li, Zhou, Peydayesh, et al., 2023). The systematic study of TS treatment on the formation of plant protein fibrils and its influence on technofunctional properties (e.g. gelation and emulsification), which are important for their application, have not been reported.

Therefore, in the present study, faba bean protein (FPI) fibrils were prepared by either TS or CH treatment. FPI was selected as a model plant protein as it is commercially available and naturally rich in all nine essential amino acids (Dhull, Kidwai, Noor, Chawla, & Rose, 2022). The impact of different treatments on the building blocks, morphology, assembly behaviour, and microstructural characteristics of FPI fibrils was investigated. The effects of fibrillisation on viscosity, viscoelasticity, and thermo-reversible gelation characteristics were also studied. Finally, O/W high internal phase emulsions (HIPEs) (soybean oil volume fraction $\varphi = 0.75$) stabilised by 3 wt% TS-induced FPI fibrils were prepared. Furthermore, rheological properties and microstructural characteristics of HIPEs were studied. This study provides valuable insights into the influence of TS treatment on the formation of amyloid-like fibrils and their structural characteristics and inform their technofunctional properties.

2. Materials and methods

2.1. Materials

The FPI was purchased from NZ Protein Inc. (Auckland, New Zealand). Based on the product specification from the manufacturer, it contains ~85 wt% protein, ~5.4 wt% fat, and ~1 wt% carbohydrate and dietary fibre, respectively. Soybean protein isolate (SPI) and pea protein isolate (PPI) containing ~85 wt% protein was obtained from Yantai T. Full Biotech company (Shandong, China). Chemicals used in this study including sodium dodecyl sulfate (SDS), NaCl, Fast Green, Nile Red, acetic acid, thioflavin T (ThT), low viscosity mineral oil (M5904), sodium cacodylate, glutaraldehyde, HCl, NaOH, sodium azide, ammonium bicarbonate, urea, thiourea, dithiothreitol (DTT), iodoacetamide (IDA), trypsin, formic acid, trifluoroacetic acid, acetonitrile, acetonitrile (MeCN), and Bradford protein assay kit were all analytical grade and purchased from Sigma-Aldrich (St. Louis, MO, USA). β-mercaptoethanol, 10 × Tris/Glycine/SDS running buffer, and Coomassie Brilliant Blue R-250 staining solution were purchased from Bio-Rad (Hercules, CA, USA). Milli-Q water (Millipore, USA) was used throughout sample preparations.

2.2. Preparation of plant protein dispersions

A stock solution of 10 wt% FPI was prepared by dispersing the FPI powder in Milli-Q water containing 0.02 wt% sodium azide to prevent microbial growth, followed by magnetically stirring (~300 rpm) at ~20 °C for 24 h for complete hydration. The pH was adjusted to 2.0 using 1 M HCl, followed by stirring (~300 rpm) for another ~24 h, and the pH was regularly checked and adjusted until stable. Afterwards, the stock FPI solution was stored at 4 °C until further use within a week. FPI dispersions of different concentrations (2.5 wt% and 3.0 wt%) were prepared by diluting the 10 wt% FPI stock solution with Milli-Q water at pH 2. SPI and PPI dispersions were also prepared according to the same procedure as FPI.

2.3. Formation of FPI amyloid fibrils by thermosonication (TS)

To investigate the formation of fibrils from plant-based protein sources, FPI dispersions (10 g each, 2.5–10 wt%, pH 2) were transferred to 20 mL glass vials and sonicated for 10 min (TS-10), 20 min (TS-20), and 30 min (TS-30) (50% amplitude, pulse durations of on-time 30 s and off-time 30 s) in a 90 °C water bath, respectively using a 20 kHz ultrasonicator equipped with a 6 mm horn with a dial power of 950 W (JY92-IIN, Ningbo Scientz Biotechnology Co., ltd, China) (Kamada, et al., 2021). The actual sonication power was determined as 14.4 W using the calorimetric method by determining the temperature increase of sonicated water (10 g) with time (Contamine, Wilhelm, Berlan, & Delmas, 1995; Luo et al., 2022). SPI and PPI fibrils were formed by the same methods as FPI (TS-30). All samples were accurately weighed before and

after TS and topped up with Milli-Q water (pH 2) to compensate for water evaporation. All FPI samples were prepared in duplicate and left at 20 °C for 24 h to allow FPI fibrils and gels formation (Hu, et al., 2019). For comparison, the conventional heat treatment without ultrasonication was also employed to form fibrils by heating the dispersions of plant proteins in an air oven (Thermo Fisher Scientific Inc., USA) at 90 °C for 1 h (CH-1), 3 h (CH-3), 4 h (CH-4), and 8 h (CH-8). FPI dispersions (2.5–10 wt%, pH 2) without any treatment are defined as controls in this study.

2.4. Characterisation of FPI fibrils

2.4.1. Thioflavin T (ThT) fluorescence spectroscopy

Thioflavin T (ThT) fluorescence assay was conducted using a fluorescence spectrophotometer (RF-6000, Shimadzu, Kyoto, Japan) to detect β-sheet structure according to Nilsson (2004) and Herneke et al. (2021) with slight modifications. Briefly, ThT solution (2 mM) was prepared in Milli-Q water and filtered with a 0.22 μm syringe filter (Thermo Fisher Scientific, USA). FPI fibril samples were diluted to 0.01 wt% with Milli-Q water (pH 2). An aliquot of FPI fibril dispersion (2 mL) was subsequently mixed with 2 μL of ThT solution and incubated at room temperature (~20 °C) for 10 min in the dark. Fluorescence intensity was measured at an excitation wavelength λ_{ex} of 440 nm and an emission wavelength λ_{em} from 460 to 560 nm. ThT working solution added with 2 mL Milli-Q water (pH 2) was measured as a background.

2.4.2. Determination of FPI fibrils conversion rate

Fibril conversion was assessed following the method outlined by Akkermans et al. (2007) and Zhou et al. (2024) with minor modifications. Briefly, diluted FPI fibril samples (5 mg/mL) were allowed to sediment on the bench overnight, then the supernatants were collected, and protein concentrations of the supernatant was determined using a Bradford protein assay kit (Sigma-Aldrich, St. Louis, MO, USA). Thereafter, the supernatant (1 mL) was passed through 2 mL centrifugal membrane filter (100 kDa MWCO, Merck Millipore Ltd, Ireland) under consecutive centrifugations at 4000 *g* for 15 min at 20 °C in order to remove small peptides and nonfibrillar proteins. The retentates were washed with Milli-Q water (pH 2) 2–3 times until no protein was detected in the filtrated solution. Then, the filtrate was collected, and the protein concentration was determined by a Bradford protein assay kit (Sigma-Aldrich, St. Louis, MO, USA). The conversion rate of FPI fibrils was calculated using equation (1):

$$C = \frac{S - F}{P} \times 100\ \% \tag{1}$$

where C is the conversion rate of FPI fibrils (%), S (g) is the protein content in the supernatant of FPI dispersion after sedimentation, F (g) is the protein content in the filtrate obtained from centrifugal filtration, and P (g) is the initial protein content (g) in the solution.

2.4.3. Negative staining transmission electron microscopy (TEM)

The morphology and microstructure of FPI fibrils were observed using negative staining TEM according to Ji et al. (2021). The protein dispersions containing 2.5 wt% protein was firstly diluted to 0.05 wt% by Milli-Q water (pH 2), and then 20 μL of sample solution was transferred onto a copper TEM grid coated with formvar and then stained with uranyl acetate (2%) for 3 min. Afterwards, the excess stain was washed with 20 μL Milli-Q water for another 3 min. Finally, the excess liquid was drained off from the copper grid by a filter paper. The microstructure of FPI fibrils was observed by a Philips electron microscope (NL-5600 MD, Philips, Eindhoven, The Netherlands) at an acceleration voltage of 60 kV.

2.4.4. Small-angle neutron scattering (SANS)

SANS experiments were performed on the QUOKKA instrument at ANSTO, Sydney, Australia, covering a Q-range from 0.003 to 0.4 $Å^{-1}$ (Gilbert, Schulz, & Noakes, 2006; Wood et al., 2018; Yang, de Campo, et al., 2022). The samples were prepared following the same procedure as described in sections 2.2 and 2.3. Approximately 1 mL samples were loaded into demountable SANS sample cells with the 1 mm path length by disposable syringes. Gel samples were first melted at 90 °C for 30 min in an oven before transferring to the SANS sample cells and then equilibrated at room temperature (~20 °C) for at least 5 h before SANS measurements to allow gel network formation. A multi-position tumbler was used to prevent sample sedimentation for liquid samples (e.g. 2.5 wt % and 5 wt% TS-30 samples). All SANS measurements were conducted at room temperature (~20 °C) for ~3 h for each measurement. Instrumental configurations were: (i) source-to-sample distance (SSD) = sample-to-detector distance (SDD) = 20 m, (ii) SSD = SDD = 8 m and (iii) SSD = 4 m and SDD = 1.3 m with 300 mm detector offset, using a λ of 5 Å with 10% resolution. There was an additional focussing optics configuration (iv) with the same SSD and SDD as (i) which was used to access lower Q_{min} with λ of 8.1 Å with 10% resolution. A sample aperture with a diameter of 12.5 mm was used for all configurations. Source aperture of 50 mm was used for (i), (ii) and (iii) and 30 mm for (iv). The data were reduced following a standard procedure (Kline, 2006) using the Igor Pro software (Wavemetrics, USA).

SANS data analysis:

SANS data were analysed using a Modelling II tool in the Irena SAS package embedded in Igor Pro 8.0 software (Wavemetrics, USA). In the low Q range ($Q < 0.005$ $Å^{-1}$), SANS data were analysed using the power law model shown in eq (2).

$$\mathrm{I}(Q) = aQ^{-n} \tag{2}$$

where a represents scale factor, and n is the power law exponent. In the mid to high Q regime ($0.005 < Q < 0.4$ $Å^{-1}$), data were modelled using an isotropically distributed cylindrical form factor (P(Q)) with radius following a log-normal distribution, as described in eq (3) (Guinier, Fournet, Walker, & Yudowitch, 1955).

$$p(Q) = \frac{Scale}{V_{cyl}} \int_0^{\pi/2} f^2(Q,\alpha) sin\ \alpha d\alpha$$

$$f(Q,\alpha) = 2\left(\rho_{cly} - \rho_{solv}\right) V_{cyl} j_0(QH\ cos\ \alpha) \frac{J_1(Qr\ sin\ \alpha)}{(Qr\ sin\ \alpha)}$$

$$j_0(x) = \frac{sin(x)}{x} \tag{3}$$

where V_{cyl} represents the volume of the cylinder. $J_1(x)$ is first order Bessel function, and α is the angle between cylinder axis and the scattering vector. H is the half length of the cylinder. ρ_{cyl} and ρ_{solv} are the neutron scattering length densities (SLDs) of the cylindrical scattering object and the surrounding solvent. During the modelling, the length of fibrils was fixed to 20000 Å and the SLD of FPI fibrils and solvent (H_2O) were 1.9×10^{-6} $Å^{-2}$ and -0.56×10^{-6} $Å^{-2}$, respectively (Zhang, et al., 2012). A log-normal radius distribution of cylinder radius D (R) can be expressed:

$$D(R) = \frac{\varphi}{\sqrt{2\pi}\sigma} \left(\frac{1}{2R}\right) exp\left\{\frac{-\left(ln\left[\frac{R'}{R'_{med}}\right]\right)^2}{2\sigma}\right\} \tag{4}$$

$$R' = R - R_{min} \tag{5}$$

$$R'_{med} = R_{med} - R_{min} \tag{6}$$

$$\sigma = ln\left(\frac{R_{med} - R_{min}}{R_{mode} - R_{min}}\right) \tag{7}$$

Where φ is the volume fraction, R_{min} is the minimum radius, R'_{med} is the modified median radius and σ is the standard deviation.

2.5. Secondary protein structure of FPI fibrils

2.5.1. Far UV-circular dichroism (CD) spectroscopy

Conformational changes of FPI secondary structures upon fibrillisations were investigated with CD spectroscopy using a Chirascan spectrometer (Applied Photophysics, UK). Samples were diluted with Milli-Q water (pH 2) to a concentration of 0.5 wt%. To remove some peptides, some samples were also purified by the same procedure as described in 2.3.1 using a 50-mL 10 kDa centrifugal filter (Merck Millipore Ltd, Ireland). The retentates were washed with Milli Q water (pH 2) three times followed by centrifugation and all the supernatants and retentates were collected. Samples (~80 μL) were subsequently transferred into a quartz cell (Hellma, Germany) with a 0.1 mm path length. Spectra were obtained at 20 °C in a wavelength range of 180–260 nm, with 1 nm steps and at 0.5 s per point, and then were averaged from 10 measurements.

2.5.2. Attenuated total reflectance fourier-transform infrared (ATR-FTIR) analysis

FTIR spectra of FPI samples were acquired using a diamond ATR-FTIR spectrometer (ALPHA II, Bruker, Germany) over a wavelength range from 4000 to 400 cm^{-1} with 4 cm^{-1} resolution by averaging over 32 scans, as based on previous studies (Kutzli, et al., 2023; Luo et al., 2022). Sample solution (5 μL) was pipetted on top of the ATR diamond and left to dry for 15 min at room temperature (~20 °C) before measurement.

2.6. Sodium dodecyl sulfate–polyacrylamide gel electrophoresis (SDS-PAGE)

SDS-PAGE under reducing conditions was used to characterise the protein profiles after different treatments based on their molecular weight (Laemmli, 1970). Diluted 0.15 wt% FPI solution (10 μL) was mixed with 10 μL of sample buffer at room temperature (~20 °C). The sample buffer consisted of 13% (v/v) 0.5 M Tris–HCl buffer, 10% (v/v) glycerol, 2% (w/v) SDS, 0.04% (w/v) bromophenol blue and β-mercaptoethanol (19:1, v/v). The sample was subsequently boiled for 10 min followed by cooling. Samples (15 μL) were then loaded onto a previously prepared SDS gel (Mini-PROTEAN II system). The gel was prepared at 16% (w/v) acrylamide concentration for the resolving gel and at 4.0% (w/v) acrylamide concentration for the stacking gel. The electrophoresis was performed using a PowerPac Basic (Bio-Rad, USA) at a constant voltage of 130 V in a running buffer (10 × Tris/Glycine/SDS running buffer) for ~1 h (Bio-Rad, USA). Afterwards, the gels were stained with Coomassie Brilliant Blue R-250 staining solution (Bio-Rad, USA) for 45 min. After destaining with 10% isopropanol/glacial acetic acid solution overnight on a shaker (OM6, RATEK, Australia), the gel was scanned by a molecular imager GelDoc XR system (Bio-Rad Laboratories, Hercules, USA). A mixture of protein standards with a molecular weight range of 2–250 kDa (Precision Plus Protein Dual Xtra Prestained Standards, Catalog #1610377, Bio-Rad, USA) was used to identify protein bands.

2.7. Liquid chromatography linked to tandem mass spectrometry (LC-MS/MS)

LC-MS/MS was used to identify the differences in peptide released between US and CH treatments on the formation of FPI fibrils according to the methods from Visser, Loo, Norris, and Parry (2023) with slight modifications. Firstly, FPI fibril dispersions were diluted to 1 wt% with Milli-Q water (pH 2) and filtered (4000×*g*, 15 min, 20 °C) using centrifugal filter units (2 mL) with a MWCO of 100 kDa (Merck Millipore Ltd, Ireland) to remove small peptides hydrolysates (Yang, Jiao, et al., 2022). The retentate was washed with Milli-Q water (pH 2) and centrifuged three times until the absorbance of filtrate at 280 nm dropped close to 0 according to Chatani et al. (2009). Retentate fibrils were lyophilised for 4 days with a Labconco freeze dryer (FreeZone 6 L Console, Labconco, USA). Lyophilised fibrils were then solubilised in 0.3 mL of 1 M ammonium bicarbonate buffer containing 6 M urea/2 M thiourea in a sonicator bath (Elma®, model EP30H) at room temperature for 10 min until completely solubilised. The solubilised proteins were centrifuged (17,000 g, 20 °C, 15 min) and 30 μl of the supernatant were transferred to clean centrifuge tubes (Protein LoBind 0.5 mL tubes, cat. # EP0030108094, Eppendorf). The samples were reduced by 10 mM dithiothreitol (DTT) (50 °C, 1 h), followed by alkylation with 15 mM iodoacetamide (IDA) in the dark at 20 °C for 30 min. Excess IDA were neutralised by adding 10 mM DTT and incubated in the dark at 20 °C for 30 min. MS grade water (Optima™ LC/MS Grade, cat. #FSBW6-4, Fisher Chemical™) was added to the reaction mixture to dilute the urea to 0.6 M for trypsin digestion. Trypsin (1 μg) (SOLu-Trypsin, cat. # EMS0004, Sigma) was added to each sample and incubated at 37 °C for 16 h. Another portion (0.5 μg) of trypsin was added to each sample after incubation and continued to incubate for another 5 h. The digestions were stopped by adding formic acid to a final concentration (1%). Samples were then centrifuged (17,000 g, 4 °C) for 15 min and filtered through a 0.45 μm filter (Millex syringe filter, PES, 13 mm, cat. # SLHPX13NK, Millipore) before transferring to HPLC vials for LC-MS/MS analysis.

The liquid chromatography (LC) system (Dionex UltiMate™ 3000 Binary RSLCnano LC system, Thermo Fisher Scientific) equipped with a 50 mm reverse phase analytical column (PepMap™100, C18, 2 μm particle size, 75 μm inner diameter, 50 cm length, Thermo Fisher Scientific) and an in-line RP-HPLC trap for desalting (PepMap™100 C18, 3 μm particle size, 75 μm inner diameter, 2 cm length, Thermo Fisher Scientific) was used in this study. The trap loading buffers were trifluoroacetic acid (TFA) (0.1 %) and acetonitrile (MeCN) (2 %) in MS-grade water with the flow rate of 15 μL/min. LC buffer A (0.1 % formic acid (FA) and 2 % MeCN) and B (0.1 % FA and 98 % MeCN) were used to efficiently separate and elute the tryptic peptides in a gradient of 3–30% B over 60 min at a flow rate of 300 nL/min. The LC system was coupled to a Q-Exactive™ Plus mass spectrometer (ThermoFisher Scientific) equipped with a higher-energy collision-induced dissociation (HCD) collision cell, an Orbitrap mass analyser and a Nano Flex ion source. MS1 scans were acquired with a resolution setting of 70,000 FWHM and fragment ion spectra produced via HCD were acquired with a normalised collision energy of 28% and a resolution setting of 17,500 FWHM. For data-dependent acquisition of HCD spectra, the top 10 most intense peptide ions within a mass range of 375–1650 m/z were fragmented to obtain their sequence information for identification. Exclusion conditions were optimised according to observed chromatographic peak width (~15 s).

Proteome Discoverer software (version 2.4.1.15, Thermo Fisher Scientific, USA) was used for data visualisation. The following search parameters were used for identification: Trypsin/P, precursor mass tolerance 10 ppm, fragment mass tolerance 0.02 Da, up to two missed cleavages were allowed, minimum peptide length of six amino acids, oxidation (M), deamination (N/Q), protein N-terminal acetylation, met-loss, and met-loss with acetylation were set as variable modifications and carbamidomethyl (C) as fixed modification. The minimal number of unique peptides for each protein identified was set to two and the false discovery rate was set at 1 % or less. Data were searched against the UniProt database (taxonomy: *Vicia faba* on 18-08-2023).

2.8. Characterisation of FPI fibrillar gels

2.8.1. Flowability of FPI fibrillar gels

To visually examine the flowability of FPI fibrillar gels, after samples preparation for 24 h at room temperature (~20 °C), the glass vials were inverted, and photographs were taken to observe the flowability.

2.8.2. Small and large oscillatory deformation rheology

Rheological properties of FPI fibrillar gels formed by different treatment methods were characterised by a stress-controlled rheometer (Physica MCR 301, Anton Paar, Austria) equipped with a parallel plate geometry (40 mm in diameter, 1 mm gap). Samples were transferred onto the bottom plate with a wooden spatula, and then carefully trimmed around the edge of the sample before covering with low viscosity mineral oil (Sigma-Aldrich, USA) to prevent evaporation. Rheological measurements were conducted according to the following protocol. Firstly, a time sweep measurement was conducted at a fixed strain (1%) and frequency (1 Hz) for 2 h to monitor fibrillar gels after sample loading. A frequency sweep test was then conducted at 1% strain while the frequency was varied from 0.01 to 100 Hz to probe the viscoelasticity of the gel network. Finally, a strain sweep test was performed at a constant frequency of 1 Hz while the strain amplitude was varied from 0.01 to 1000%. The storage modulus G' and loss modulus G'' were recorded throughout the tests (Hu, Cheng, Lee, & Yang, 2023). To determine the thermoreversibility of TS-30 gel, a temperature sweep with a heating and cooling rate of 2 °C/min at a fixed strain 1% and a constant frequency of 1 Hz was conducted from 20 °C to 80 °C and held at 80 °C for 10 min and subsequently from 80 °C to 20 °C to obtain the gelation temperature and melting temperature, respectively.

2.8.3. Viscosity determinations

The viscosity was measured by the same rheometer and geometry used in the oscillatory deformation test. The measurement was performed by applying a shear rate sweep from 0.1 to 1000 s^{-1} followed by a reverse sweep from 1000 to 0.1 s^{-1}. The extent of the protein aggregation can be determined by the area (S) of the hysteresis delimited by the up and down curves, calculated by Origin Pro software (version 2020, Origin Lab, MA, USA) (Luo, Zhang, Palmer, Hemar, & Yang, 2021). All measurements were performed in duplicate at 20 °C.

2.8.4. Scanning electron microscopy (SEM)

The methods for SEM sample preparation and images were based on Goeden-Wood, Keasling, and Muller (2003) with modifications. Gels were firstly cut into small pieces using a spatula and were then fixed in 0.1 M sodium cacodylate phosphate buffer containing 2.5% glutaraldehyde overnight at 4 °C. Fixed gels were washed three times with 0.1 M sodium cacodylate phosphate buffer. After washing, gels were dehydrated in a series of aqueous ethanol solutions (30%, 50%, 70%, 80%, 90%, and 100% ethanol, v/v). Dehydrated gels were frozen by liquid nitrogen and then freeze-dried for 48 h. Finally, gels were cut to approximately 1 mm × 1 mm in size and placed in a sample holder. The samples were coated with gold for 240 s at 12 mA at a temperature of ~20 °C. Images were taken by a scanning electron microscope (Philips XL 30S FEG, Eindhoven, The Netherlands) at 5 kV.

2.9. Formation and characterisation of high internal phase emulsions (HIPEs)

2.9.1. Interfacial tension measurements

The interfacial tension of oil droplets in FPI fibrils (0.1 wt%) was conducted through a Theta Flex Plus optical tensiometer (Biolin Scientific Instruments, Sweden) with the pendant drop method (Hu, et al., 2023). An FPI fibril solution (25 μL) was generated at the stainless-steel syringe tip and immersed in soy oil, and interfacial tension changes with time were monitored up to 6000 s and calculated automatically by One Attention software (Biolin Scientific Instruments, Sweden).

2.9.2. Preparation of HIPEs

HIPEs were prepared by homogenising TS-30 FPI fibril solution (3%, w/w) with soybean oil at oil-phase volume fractions (φ) of 75% (v/v) using a high shear mixer (T10 basic ULTRA-TURRAX®, IKA Corp., Staufen, Germany) with a 10 mm probe (S10N-10 G, IKA, Germany) at a speed of 14, 500 rpm for 2 min. After homogenising, a semi-solid HIPE was formed. HIPE prepared by the same procedure with 3% FPI (w/w) solution without any treatment was used as a control.

2.9.3. Oil droplet size

The mean particle size and particle size distribution (PSD) of oil droplets in HIPEs were measured by a static laser light diffraction technique (Mastersizer 2000; Malvern Instruments Ltd, Worcestershire, UK) according to Hu et al. (2023). The refractive indices used for soybean oil and the dispersant (Milli-Q waster) were 1.47 and 1.33, respectively (da Silva, Almeida, & Sato, 2021). The Sauter mean diameter (D [3,2]) was used to represent mean particle diameter for oil droplets.

2.9.4. Confocal laser scanning microscopy (CLSM) of HIPEs

For CLSM sample preparations, Fast Green (1% w/v) and Nile Red were used to stain protein and oil phases with a ratio of 500:1 (v/v) and 5000:1 (v/w), respectively (Hu, et al., 2023). Once HIPEs were made, aliquots of samples were added into a glass slide with a cavity covered with a coverslip and sealed by nail polish to prevent water evaporation. The HIPE samples were observed with a confocal laser scanning microscope (Leica DM 6000B, Germany) equipped with an oil immersed 100 × objective lens at laser wavelengths of 633 nm for Fast green and 561 nm for Nile red. All images were processed using Image J software (NIH, MD, USA).

2.9.5. Rheological measurements of HIPEs

Rheological measurements were conducted according to the same methods as described in section 2.8.2. All data were collected at 20 °C. Storage modulus (G') and loss modulus (G'') were recorded during the frequency sweep (0.01–100 Hz, 1% strain) and strain amplitude tests (0.1–1000%, 1 Hz).

2.10. Statistical analysis

All the experiments were conducted at least in duplicate, and the results are reported as mean ± standard deviation (SD). All data were analysed using Minitab statistical software (Minitab 19 Statistical Software, USA). The one-way analysis of variance (ANOVA) was applied to analyse the data. The difference between sample mean values was evaluated via a Tukey's test at a significance level of $P < 0.05$.

3. Results and discussion

3.1. Visual appearance, ThT fluorescence, and microstructures of FPI fibrils

3.1.1. Visual appearances of FPI dispersions and gels

The appearances of FPI fibril solutions (2.5 wt%) and gels (10 wt%) prepared from different treatments are shown in Fig. 1A. For 2.5 wt% FPI, control and CH treated samples are highly turbid and protein sedimentation at the bottom of glass vials was clearly observed (indicated by red arrows in (Fig. 1A). This was due to the low water solubility of plant protein and heat induced protein aggregation (Alavi, Chen, & Emam-Djomeh, 2021; Alavi, Chen, Wang, & Emam-Djomeh, 2021). After the TS treatment for 10–30 min, FPI dispersions became translucent indicating a significant improvement in solubility. Similar observations have been made in previous studies of mung bean protein isolate dispersion (10 wt%) (Zhong & Xiong, 2020) and SPI dispersions (10 wt%) after TS treatment (5–30 min and 30–90 °C) (Kamada, et al., 2021). It was reported that ultrasound could help the infiltration of the protein with water so that the solubility can be improved (Frydenberg, Hammershøj, Andersen, Greve, & Wiking, 2016). Fibrillar gels can be observed in TS-20 and CH-4 samples (10%, w/w), and the TS-induced gels were more transparent than CH-induced gels (Fig. 1A). These results also showed that the CH treatment required longer time (>3 h) to induce self-supporting gels than the TS treatment, which only needs 20

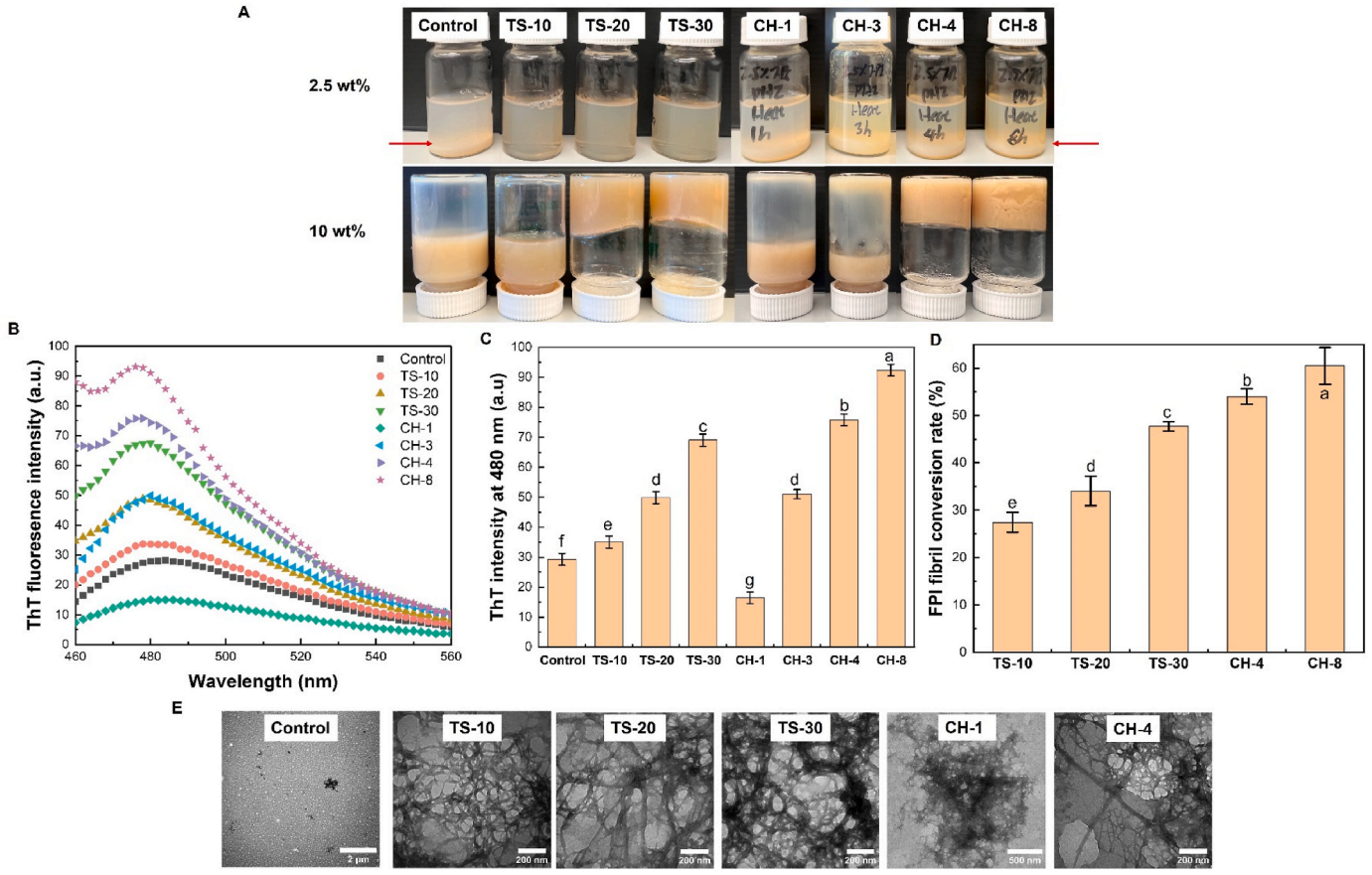

Fig. 1. (A) Visual appearance of 2.5 wt% and 10 wt% faba bean protein isolate (FPI) samples after thermosonication (TS) and conventional heat treatment (CH) for different time at pH 2. (B) ThT fluorescence spectrum of FPI dispersions before and after TS (10, 20, and 30 min) or CH (1, 4, and 8 h) treatment at pH 2. (C) ThT fluorescence intensity at 480 nm at pH 2 as function of different treatment and time. (D) FPI fibril conversation rate (%) as function of different treatment and time. (E) TEM images of FPI fibrils (2.5 wt %) formed after TS (10, 20, and 30 min) and CH (1 and 4 h) at pH 2. All samples were extensively diluted to ~0.05 wt% prior to TEM observations. Different letters above the columns indicate significant difference ($P < 0.05$).

min (Fig. 1A). Rheological properties and microstructural characteristics of FPI gels induced by different treatments are discussed in section 3.4.

3.1.2. *Thioflavin T (ThT) fluorescence assay*

The ThT fluorescent dyes can specifically bind to the β-sheet structures in protein fibrils, so ThT fluorescence has been widely used to detect protein fibril formation by measuring the increase of fluorescence intensity (Biancalana and Koide, 2010; Wang et al., 2023). The ThT fluorescence spectra of FPI sample before and after various CH or TS treatments are shown in Fig. 1B. The results shows that the TS or CH treatment (except for CH-1) resulted in a significant increase in ThT fluorescence compared to control, indicating the formation of β-sheet rich fibrillar structures (Xu et al., 2023). The peak fluorescence intensity at 480 nm of all samples is plotted in Fig. 1C. For both TS and CH treated samples, an increase in treatment time led to an increase in fluorescence intensity at 480 nm, demonstrating a time-dependent fibrillisation kinetics. Even after 10 min TS, FPI proteins showed a significantly higher ThT intensity than the control groups, and the maximum intensity increased with the increasing TS time from~35 at TS10 to ~69 at TS30 (Fig. 1C). A similar trend was also found in the CH samples, which showed that heating for longer time led to greater ThT intensity, increasing from ~16 (CH-1) to ~92 (CH-8). Notably, TS-20 sample had a comparable ThT intensity at 480 nm (~50) compared to CH-3 samples (~51), indicating a similar extent of fibrillisation (Yang, Jiao, et al., 2022). The similar increase of ThT fluorescence intensity with heat treatment time during fibrillisation has been also reported in other proteins, such as WPI, SPI, and PPI (Biancalana and Koide, 2010; Wang et al., 2023; Zhang and Dee, 2023). The results also indicated that the TS treatment accelerated formation of FPI fibril formation compared to the CH treatment. The lowest ThT fluorescence intensity observed in the CH-1 sample could be attributed to the protein aggregation making less surface area available for ThT binding (Jo, Huang, & Chen, 2020; Josefsson et al., 2019).

3.1.3. *Analysis of fibril conversion rate*

The relative conversion rate of the FPI fibrils after different treatments and time is shown in Fig. 1D. Among all the samples, the maximum FPI fibril conversion was found at CH-8 (~60%), followed by CH-4 (~53%) and TS-30 (~47%). In either TS or CH treated FPI samples, the extent of fibril conversion rate increased with an increase in treatment time. Similar trend can also be found in Yu et al. (2024) and Sun, Wang, Xiong, and Fang (2021), who reported that acidic heating at longer time resulted in a greater protein fibril conversion rate. Furthermore, it is worth noting that only a limited portion of FPI were involved in fibrillation induced by either TS or CH treatment, and other proteins may exist as peptides or amorphous protein aggregates (Cao & Mezzenga, 2019; Zhang et al., 2023). In addition, the FPI fibril conversion rate results generally agree well with the ThT fluorescence findings (Fig. 1C). Similar findings have been reported in previous studies on other food protein fibrillizations, such as SPI fibrils (Yu, et al., 2024) and WPI fibrils (Bolder, Sagis, Venema, & van der Linden, 2007).

3.1.4. Morphology of FPI fibrils as revealed by TEM

TEM images of FPI samples before and after TS or CH treatment are displayed in Fig. 1D. In the control FPI sample, the presence of submicron particle aggregates was observed. However, after only 10 min of TS treatment, long, straight, and interconnected FPI fibrils with a diameter of approximately 5–12 nm are clearly visible. Similar fibril morphologies have been observed in a previous TEM study of soy protein isolate fibrils included by the TS treatment (90 °C, 30 min) (Kamada, et al., 2021). With increasing TS treatment time to 20 and 30 min, a larger number of fibrils with a more compact and more entangled fibril network can be observed. This finding agrees well with ThT fluorescence results that longer TS treatment induced an increase in the amount of β-sheet in the protein fibrils (Fig. 1C). In addition, TS treatment (90 °C for 30 min at pH 2) is also effective in fibrillisation of other plant proteins such as SPI and PPI (Fig. S1). For the CH-treated sample, the morphology of FPI fibrils underwent significant changes during the CH treatment. There was only large amorphous protein aggregate with short fibrils formed at a shorter acidic heating time (e.g. 1 h in CH-1 sample). This was also consistent with its low ThT fluorescence (Fig. 1C). After the acidic heating for a longer time (CH-4), the formation of fibrils with a well spanned network was observed. The morphologies of FPI fibrils induced by TS or CH treatment as shown in Fig. 1D agree well with previous studies of fibrils derived from plant proteins including faba bean protein (Herneke, et al., 2021), hemp proteins (Kutzli, et al., 2023) and rice bran proteins (Zhang & Huang, 2014). In summary, compared to traditional fibrillisation approaches such as prolonged heating, TS treatment under acidic conditions (pH 2) could significantly accelerate the fibrillisation of plant proteins (Fig. 1D and Fig. S1). This is likely due to the reduction of the high free-energy barrier by ultrasound, which is the most limiting factor to form protein fibrils (So, et al., 2011). Although the mechanism of TS induced protein fibrillisation has received limited attention in the literature, US has been proved to regulate protein fibrillisation through the transient cavitation (Nakajima, et al., 2017) and the increased surface hydrophobicity of proteins (Hu & Li, 2021).

3.2. Small-angle neutron scattering (SANS) analysis

The TEM images shown in Fig. 1D only provide a local view of fibril microstructures and may involve in artefacts problems during sample preparation (Chen, et al., 2016; Verkade, 2012). To obtain more statistically representative structural information, SANS was applied to probe the microstructures of TS-induced FPI fibrils at various concentrations and treatment times (Fig. 2). The SANS profile was fitted with a dilute rigid cylinder model (equation (2)) and the structural parameters obtained from fitting are listed in Table 1. It should be noted that the fibril length L is too large to be determined by the SANS setup used in the current study, therefore only the radius of the fibrils was determined. The radius of 2.5 wt% FPI fibrils slightly increased from ~4.3 nm to ~5.5 nm when the TS treatment time increased from 10 min to 30 min. This result agrees well with the TEM observation that longer treatment led to thicker bundle formation from stacking of fibrils (Fig. 1D). It has been reported that once the monofibrils created initially, they arrange themselves in close proximity to each other to form thicker and more expansive fibril bundles (Aggeli, et al., 2001; Mihara, Matsumura, & Takahashi, 2005; Rubinov et al., 2012). However, the radius of fibrils kept nearly constant ~5.3–5.5 nm for different concentrations of FPI, indicating FPI concentration has limited impact on the radius of fibrils formed by TS-30 treatment. Generally, the fibril radius calculated from SANS analysis matched the average single fibril radius observed by TEM and also previous studies of FPI fibrils induced by conventional heating (e.g. AFM height: 2.7–5.3 nm) (Herneke, et al., 2021; Herneke, Lendel, Karkehabadi, Lu, & Langton, 2023). In the low Q regime ($0.0008 < Q$ ($Å^{-1}$) < 0.005), the scattering intensity follows a power law decay $I(Q) \sim Q^{-n}$. The expected power law exponent n for long cylindrical fibrils is $n = 1$. However, all FPI fibrils had power law exponent (n) derived from 1 in the low Q region. For example, $n = 1.47$ (TS-10) and 1.35 (TS-30) for 2.5 wt% FPI fibrils and $n = 1.36$ for 5 and 10 wt% FPI fibrils formed

Table 1
SANS model fit structural parameters of faba bean protein isolate (FPI) fibrils and fibrillar gels formed at different FPI concentrations (2.5 and 10 wt%) and thermosonication time (10 and 30 min).

Samples	Power law exponent, n	Mean radius (nm)	Standard deviation, σ
	$Q < 0.005$ Å^{-1}	$0.005 < Q < 0.4$ Å^{-1}	
2.5 wt% FPI-TS-10	1.47 (0.03) [a]	4.3 (0.1)	0.56 (0.02)
2.5 wt% FPI-TS-30	1.35 (0.03)	5.5 (0.1)	0.38 (0.03)
5 wt% FPI-TS-30	1.36 (0.02)	5.3 (0.2)	0.39 (0.02)
10 wt% FPI-TS-30	1.36 (0.03)	5.4 (0.2)	0.37 (0.03)

[a] Numbers in parentheses represent σ error bars (or 68.3% confidence levels).

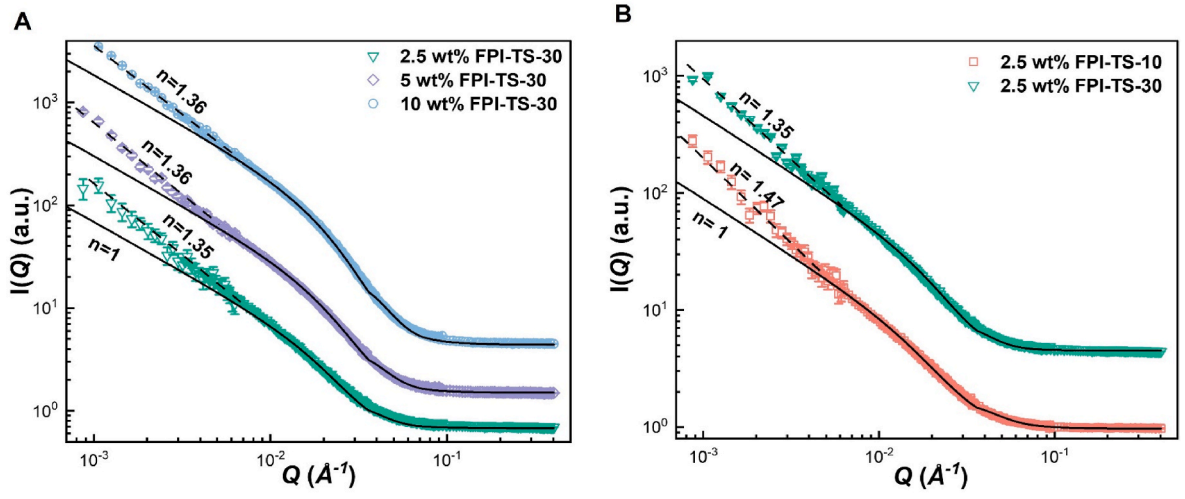

Fig. 2. Small-angle neutron scattering (SANS) profiles of (A) Faba bean protein isolate (FPI) fibrils induced by thermosonication (TS) treatment for 30 min at pH 2 at various FPI concentrations (2.5, 5, and 10 wt%). (B) FPI fibrils (2.5 wt%) induced by TS for 10 min and 30 min. Scattering profiles in (B) were arbitrarily vertically shifted for clarity. The solid black lines are the ling-cylinder form factor fits to the scattering data (eq (3)). Deviations observed between the experimental scattering data and the extrapolated fit around $Q < 0.005$ Å^{-1} are attributed to fibril-fibril interactions.

by TS-30 treatment. This could be attributed to the attractive fibril-fibril interactions and entanglements (Stanley, Perevozchikova, & Berthelier, 2011) that have been observed in a previous SAXS study of α-synuclein fibrils (Pogostin, Linse, & Olsson, 2019) and a SANS study of amyloid β peptide fibrils (Lattanzi, et al., 2021). This finding also agrees well with the TEM observations of extensive fibril-fibril interaction and entanglements in TS induced FPI fibril samples (Fig. 1D).

3.3. Secondary protein structure of FPI fibrils revealed by CD and FTIR

The secondary protein structure changes of FPI upon fibrillisation can be determined by far-UV circular dichroism (CD) and FTIR. Fig. 3A and B shows the CD spectra in the far-UV region (190–260 nm) of FPI before and after TS and CH treatment for various times. The spectrum of untreated FPI (Control) showed a negative peak around 205 nm with a small shoulder peak located ~220 nm. This suggests that secondary structure of native FPI is dominated by random coil and α-helix with a small portion of β-sheet (Greenfield, 2006). This agrees well with a previous CD study of FPI (Husband, Wilde, Clark, Rawel, & Muschiolik, 1994). It can be seen that the peak shifted only slightly from 205 nm to ~208 nm in the CH-1 sample, indicating limited conformational changes of FPI after 1 h conventional heating. However, with increasing treatment time to 4 h in CH samples, the negative peak of FPI at ~205 nm shifted to ~216 nm accompanied with a significant increase in magnitude as well, indicating the formation of β-sheet structure (Greenfield, 2006; Kutzli et al., 2023). Similar findings were found in all TS treated samples with prominent negative peaks appearing around ~218–220 nm, which demonstrated that the TS treatment even for a shorter time (10–30 min) is highly efficient in promoting secondary protein structural changes in FPI. This finding is in line with the results of ThT fluorescence as shown in Fig. 1C. Formation of β-sheet structures has been widely reported in a broad range of proteins during fibrillisation by using different methods such as β-lactoglobulin fibrils induced by microwave treatment (Hettiarachchi, Melton, Gerrard, & Loveday, 2012), WPI treated by hydrothermal treatment (Yang, Jiao, et al., 2022), and hemp proteins treated by conventional heat treatment (Kutzli, et al., 2023), suggesting that amyloid fibrils are typically rich in β-sheet structures.

It is worth noting that in the sample obtained from prolonged heating (e.g. CH-8), the negative peak was centred ~215 nm with a decrease in magnitude compared to CH-4 sample. This could be due to the fact that both amyloid fibrils and released peptides contribute to the final CD signal (Josefsson, et al., 2019; Kutzli et al., 2023), thus making the interpretation the complex CD spectrum more difficult. This becomes more prominent in CH-8 sample as more hydrolysed peptides are released as identified by SDS-PAGE (Fig. 4). The similar issue has been reported in a previous study of hemp protein fibrils (Kutzli, et al., 2023). Therefore, selected samples (TS-30 and CH-4) were further studied after purification and removing hydrolysed peptides (Fig. 3B). The filtrate fractions of both samples containing a large proportion of hydrolysed peptides that did not participate in fibril formation showed characteristics of a random coil structure with the minimum ~195 nm (Fig. 3B) (Greenfield, 2006). In terms of the purified fractions (retentates), a significant shift of this minimum from ~195 nm to ~228 nm–~232 nm was observed. Further, the peak became narrow compared with unpurified samples (Fig. 3B). Similar results have been reported in

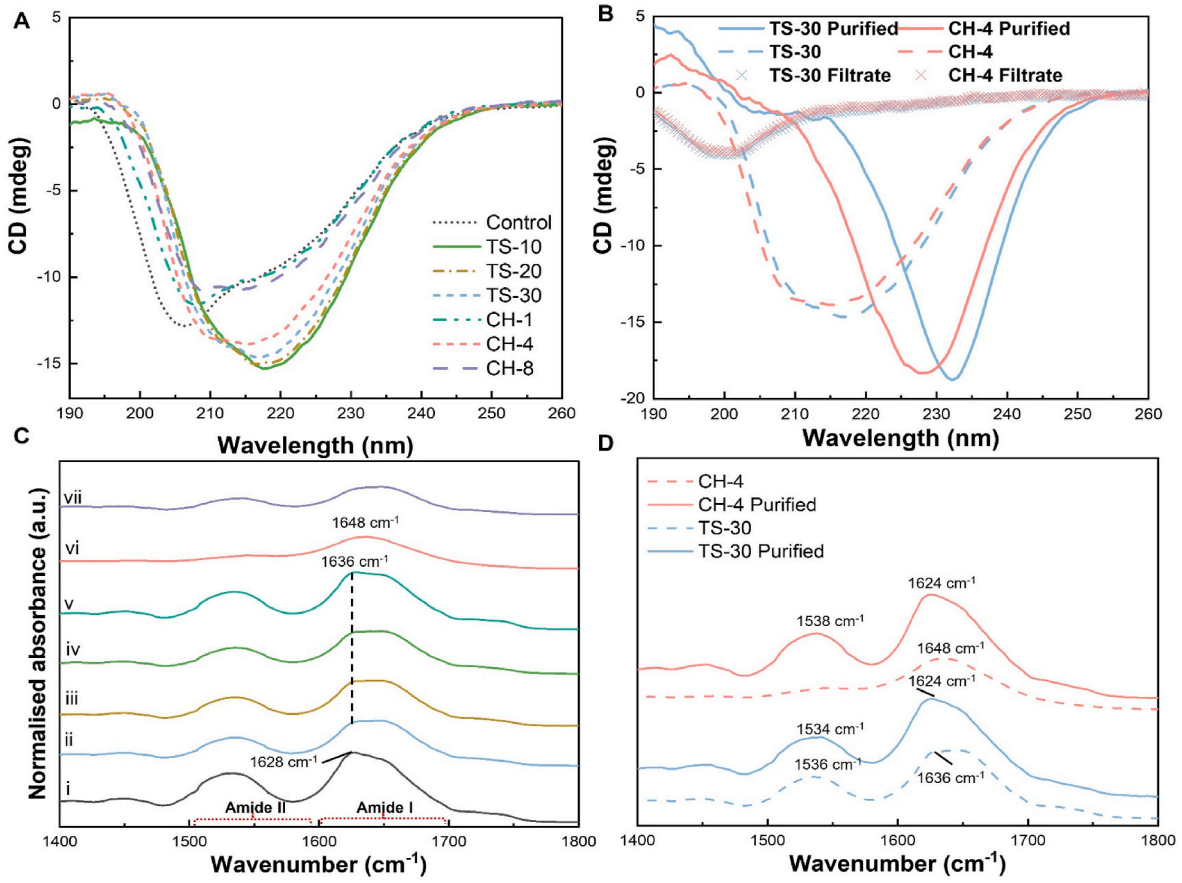

Fig. 3. Secondary structural characterisations of faba bean protein isolate (FPI) before and after thermosonication (TS) (10, 20, and 30 min) and conventional heat treatment (CH) (1–8 h) at pH 2. (A) Far ultraviolet (UV) circular dichroism (CD) spectra; (B) CD spectra of purified fibrils (retentates) and filtrates of selected samples (TS-30 and CH-4). (C) Amide I and II regions of the FTIR spectra ((i) Control, (ii) TS-10, (iii) TS-20, (iv) TS-30, (v) CH-1, (vi) CH-4, and (vii) CH-8). (D) Amide I and II regions of the FTIR spectra of purified fibrils (retentates) and filtrates of selected samples (TS-30 and CH-4).

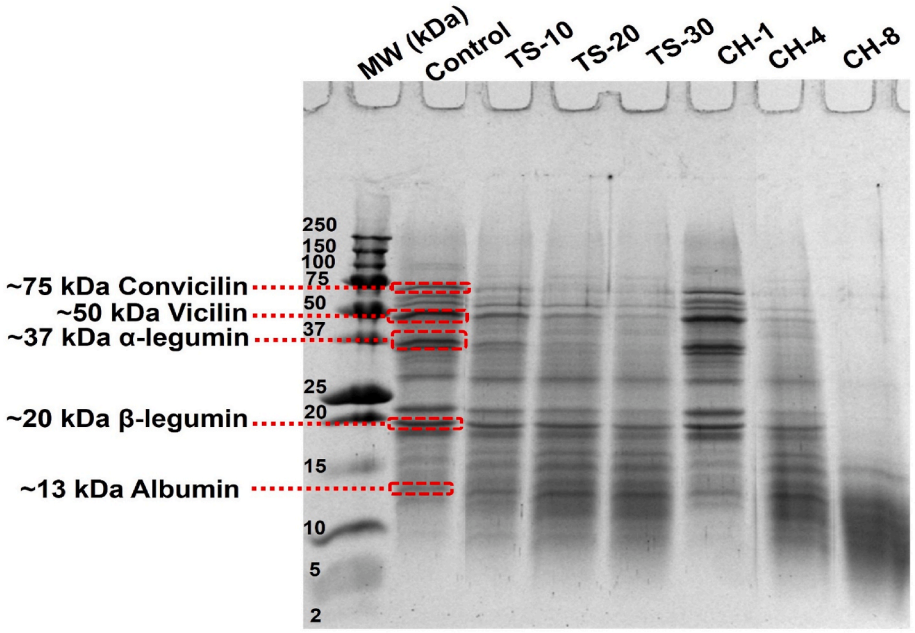

Fig. 4. SDS-PAGE profiles of the faba bean protein isolates (FPI) at pH 2 before and after thermosonication (TS) (10, 20, and 30 min) or conventional heat treatment (CH) (90 °C, 1 h, 4 h, and 8 h) under reducing conditions.

previous CD studies of potato protein fibrils and hemp protein fibrils (Josefsson, et al., 2019; Kutzli et al., 2023).

Complementary to CD, FTIR was also used to study protein secondary structures of FPI fibrils induced by different treatment. Fig. 3C shows the FTIR spectra of untreated and CH/TS treated FPI samples in amide I and II regions. According to Arrondo, Muga, Castresana, and Goñi (1993), the amide I IR band (1600–1700 cm^{-1}) provides information on the C=O and C–N stretching vibrations, and the amide II region (1470–1570 cm^{-1}) contains in-plane stretching vibrations of the C–N and C–C groups as well as the N–H bending. The FPI control sample shows a prominent peak ~1628 cm^{-1} in amide I and ~1543 cm^{-1} in amide II. Similar IR spectral features can be observed in previous FTIR studies of FPI (de la Rosa-Millán, Orona-Padilla, Flores-Moreno, & Serna-Saldívar, 2018; Martínez-Velasco, et al., 2018). After TS or CH treatment, the peak in amide I area was shifted to a higher wavenumber (~1636 cm^{-1} for TS-10, 20, 30 and CH-1 and 1648 cm^{-1} for CH-4 and 8), but the peaks in the amide II band region did not show a significant change for all samples (~1543 cm^{-1}). Previous FTIR studies demonstrated that the protein fibrillisation typically resulted in a shift of the amide I bands towards lower wavenumbers at ~1615-1630 cm^{-1}, due to a transition of protein secondary structure from random coil to β-sheet (Arrondo, et al., 1993; Zhou et al., 2022). However, the opposite observation was made here which could be attributed to the extensive overlapping of other component bands of random coils (~1645 cm^{-1}), α-helices (~1654 cm^{-1}), and β-turns (~1681 cm^{-1}) in the amide I region (Hong et al., 2011; Kutzli et al., 2023). Similar observations have been found in the CD spectra (Fig. 3A) along with the previous FTIR studies of fibrils made from hemp proteins (Kutzli, et al., 2023). Therefore, to better resolve the protein secondary structural changes from FTIR spectra, TS-30 and CH-4 samples were purified to remove hydrolysed peptides (Fig. 3D). Compared to the unpurified samples, the amide I peak of the purified amyloid fibrils shifted from ~1636 cm^{-1} (TS-30) and ~1648 cm^{-1} (CH-4) towards much lower wavenumbers of ~1624 cm^{-1}, representing significant changes in protein secondary structure from random coil to β-sheets, in line with the CD results. A similar findings have been reported in the FTIR study of SPI fibrils upon self-assembly after TS treatment (90 °C, 30 min) in 30%v/v acetic acid solution (Kamada, et al., 2021).

3.4. Characterisation of FPI fibrils

3.4.1. SDS-PAGE

SDS-PAGE was conducted to investigate the protein hydrolysis in FPI induced by different treatments (i.e., TS and CH) (Fig. 4). The control FPI sample exhibited numerous major protein bands at approximately ~75 kDa (convicilin), ~50 kDa (7S vicilin), ~37 kDa (α-legumin), and ~20 kDa (β-legumin), representing the typical protein profiles of FPI (Hu, et al., 2023; Vogelsang-O'Dwyer et al., 2020). Except for the control sample, all protein bands (>20 kDa) were gradually degraded to lower molecular weight (<20 kDa). As a consequence, the bands corresponding to peptides less than 10 kDa showed significantly increased intensity from TS-20, TS-30, CH-4, and CH-8 samples, indicating the partial hydrolysis of FPI after TS and CH at pH 2. Such hydrolysis has been widely reported during protein fibrillisation, such as WPI (Yang, Jiao, et al., 2022) and PPI (Yi, He, Peng, & Fan, 2022). In both FPI samples treated with TS and CH, the density of protein bands corresponding to convicilin, vicilin, α-legumin, and β-legumin decreased with an increase in the treatment time, similar to the hydrothermal method-induced WPI fibrils at pH 2 where longer hydrothermal time led to greater hydrolysis (Yang, Jiao, et al., 2022). The extent of protein band degradation was comparable between the TS-30 and CH-4 samples, indicating similar efficiencies in FPI hydrolysis (Fig. 4). Conversely, the CH-8 sample showed the greatest protein degradation, suggesting that prolonged heating contributed to a much higher protein hydrolysis level. These results indicated that the TS treatment was efficient in the hydrolysis of FPI proteins to peptides or polypeptides, which is a critical prerequisite for fibril formations, indicating the hydrolysed peptides acting as building blocks for the protein fibrils (Yang, Jiao, et al., 2022).

3.4.2. LC-MS/MS analysis

3.4.2.1. Identification of the peptide building blocks in FPI fibrils. For further identification of the building blocks (peptides) of FPI fibrils, TS-30 and CH-4 samples were selected for characterisation by LC-MS/MS. As shown in Fig. 5A, a large number of peptides were identified from both samples by mass spectrometry separated by high-performance liquid chromatography (LC). Comparing the data with the Uniprot protein database (https://www.uniprot.org/), there were 275 peptides

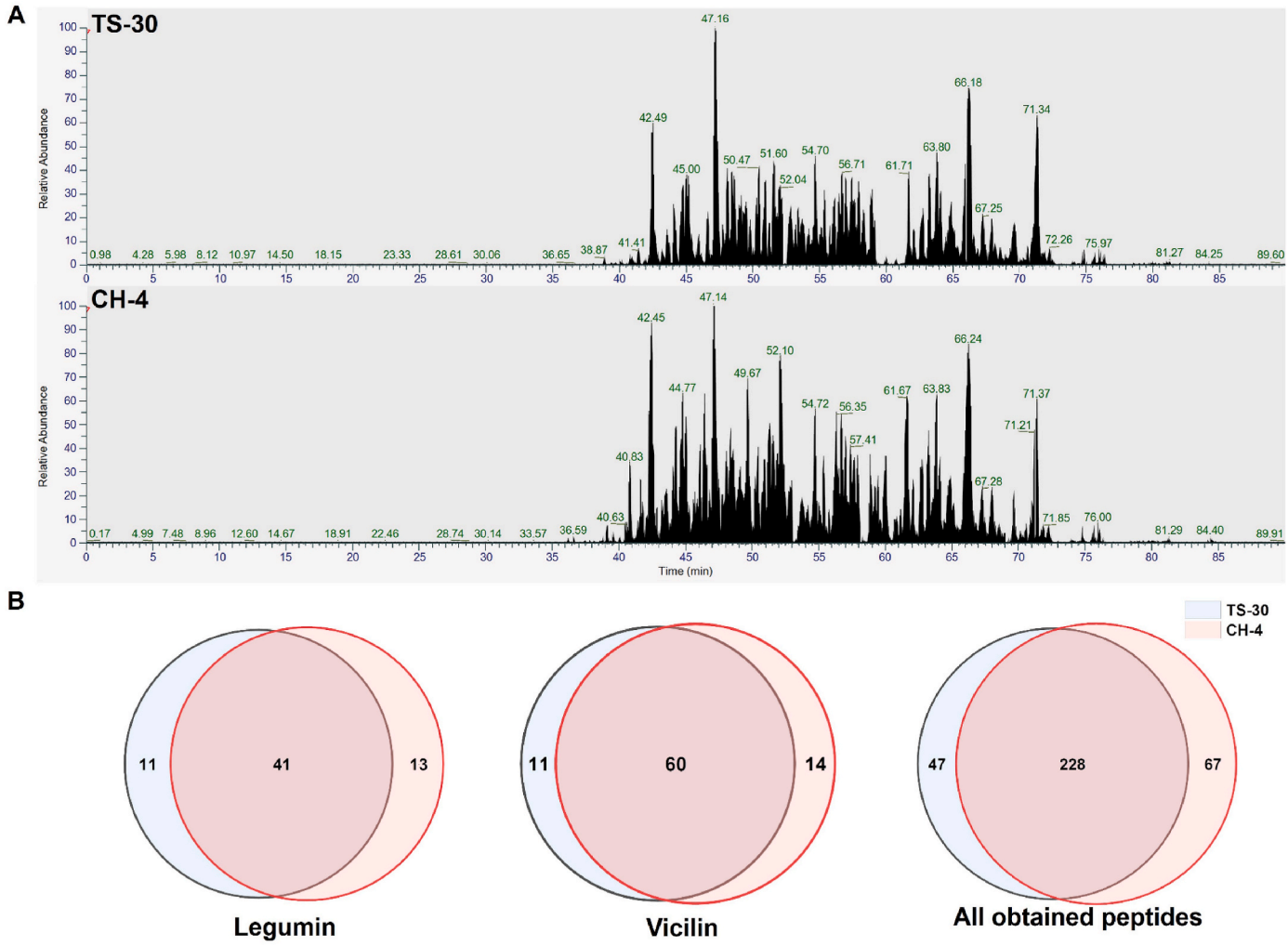

Fig. 5. (A) Basepeak peaks of faba bean protein isolates (FPI) fibrils induced by thermosonication for 30 min (TS-30) and conventional heat treatment for 4 h (CH-4). (B) Venn diagram of peptide sequences derived from legumin, vicilin, and all FPI fibrils after hydrolysis under TS-30 and CH-4 treatment. The numbers represent the number of peptides in the corresponding circle.

and 295 peptides identified in TS-30 and CH-4 fibril samples, respectively (Table S1). The Venn diagram (Fig. 5B) displays the overlap in peptide sequences of FPI fibrils prepared by TS-30 and CH-4 treatment. Despite 228 building block peptides induced by TS-30 and CH-4 treatments were identified to be in common, some unique peptides were still be detected in different treatments (Fig. 5B). For example, there were 47 and 67 unique peptides identified in the TS-30 and CH-4 samples, respectively. As revealed by SDS-PAGE (Fig. 4), legumin and vicilin were the two major proteins in FPI, therefore, peptides derived from hydrolysis of these two proteins by TS and CH treatment were also compared in Fig. 5B. There was a total of 52 (TS-30) and 54 (CH-4) peptides derived from legumin, where 41 peptides were the same, and 11 peptides were only identified in TS-30. As for vicilin, there are 71 and 74 peptides found in TS-30 and CH-4 samples, respectively with 60 identical peptides found between the two treatments. In addition, TS-30 and CH-4 samples had 11 and 14 unique peptides, respectively. Distinctive building block peptides of protein fibrils formed by different treatment methods have also been reported in previous studies. For example, Yang, Jiao, et al. (2022) reported that there were 102 and 48 unique peptides identified in WPI fibrils formed by conventional heating (90 °C for 10 h, pH 2) and using a hydrothermal method (110 °C for 4 h, pH 2), respectively. Combined with SDS-PAGE results, it can be clearly seen that the hydrolysis of proteins to small peptides are critical prerequisite steps for subsequent assembly and fibril formation induced by both CH and TS treatment (Meng, et al., 2022). The high efficiency of TS induced FPI fibrillisation could be partially attributed to the rapid hydrolysis of proteins under ultrasonication at elevated temperatures (Yang, Jiao, et al., 2022).

3.4.2.2. WALTZ and TANGO analysis of FPI fibrils. To further understand the assembly behaviour of peptide building blocks to fibrils, WALTZ (Maurer-Stroh, et al., 2010) was utilised to compute polypeptide sequences with amyloidogenic potentials and compared with the potential amyloidogenic regions in two major proteins of FPI, namely legumin and vicilin. In recent years, several algorithms such as WALTZ and TANGO have been widely used for identification of amyloid-forming sequences in proteins (Li, Zhou, Wu, et al., 2023; Maurer-Stroh, et al., 2010). Table 2 shows the amyloidogenic regions in legumin and vicilin identified by WALTZ compared to detected peptide sequences of fibrils formed by TS-30 and CH-4 treatment. For legumin (Table 2A), both TS and CH treatments could generate peptides that match with predicted amyloidogenic core regions of fibrils including LAQTFNTE and NSLLYVIR. For examples, TS-30 and CH-4 treatments generated 3 and 8 peptides respectively that contained the predicted sequence LAQTFNTE. In terms of vicilin, WALTZ predicted 7 peptides amyloidogenic potential regions (Table 2B). After matching with the detected sequences (Table S1), TS-30 treatment and CH-4 treatment generated 11 and 10 peptides, respectively containing 4 predicted

Table 2
Comparison of amyloidogenic core regions from legumin (A) and vicilin (B) in faba bean protein isolates (FPI) predicted by the algorithm WALTZ with the LC-MS/MS detected peptide sequence in FPI fibrils formed by conventional heating treatment (4 h) or thermosonication (30 min).

A

Legumin				
Hypothesised sequences	Measured sequence (TS-30)	Measured sequence (CH-4)	Location	Molecular mass (Da)
PYWTYN	–	–	–	–
LAQTFNTE	–	FSSEFLAQTFNTEEDTAKR	91–109	2221.04
	GFSSEFLAQTFNTEEDTAKR	GFSSEFLAQTFNTEEDTAKR	90–109	2278.06
	–	GGQHQQEEESEEQKDGNSVLSGFSSEFLAQTFNTEEDTAK	69–108	4414.94
	–	GGQHQQEEESEEQKDGNSVLSGFSSEFLAQTFNTEEDTAKR	69–109	4574.05
	RGGQHQQEEESEEQKDGNSVLSGFSSEFLAQTFNTEEDTAK	RGGQHQQEEESEEQKDGNSVLSGFSSEFLAQTFNTEEDTAK	68–108	4574.05
GLRIINP	–	–	–	–
NSLLYVIRG	INANSLLYVIRGEGR	INANSLLYVIRGEGR	220–234	1675.91
	–	LYRNGIYAPHWNINANSLLYVIRGEGR	208–234	3159.66
	NGIYAPHWNINANSLLYVIRGEGR	NGIYAPHWNINANSLLYVIRGEGR	211–230	2328.22

B

Vicilin				
Hypothesised sequences	Measured sequence (TS-30)	Measured sequence (CH-4)	Location	Molecular mass (Da)
NLQNYRLLEYK	LLENLQNYRLLEYK	LLENLQNYRLLEYK	66–79	1809.97
	SKLLENLQNYRLLEYK	–	–	–
ADFILVVLSG	ADFILVVLSGK	ADFILVVLSGK	93–103	1161.69
	–	DADFILVVLSGK	92–103	1276.71
	SKPHTIFLPQQTDADFILVVLSGK	SKPHTIFLPQQTDADFILVVLSGK	80–103	2654.46
	TDADFILVVLSGK	TDADFILVVLSGK	91–103	1377.76
	TIFLPQQTDADFILVVLSGK	TIFLPQQTDADFILVVLSGK	84–103	2205.22
	PQQTDADFILVVLSGK	–	88–103	1730.93
VIVKIS	–	–	–	–
KFFEI	–	FGKFFEITPK	267–276	1213.66
	SREPIYSNKFGKFFEITPK	SREPIYSNKFGKFFEITPK	258–276	2288.21
QDLNIFVNYVEIN	NPQLQDLNIFVNYVEINEGSLLLPHYNSR	NPQLQDLNIFVNYVEINEGSLLLPHYNSR	278–306	3399.73
	RNPQLQDLNIFVNYVEIN	–	277–294	2189.13
	RNPQLQDLNIFVNYVEINEGSLLLPHYNSR	RNPQLQDLNIFVNYVEINEGSLLLPHYNSR	277–303	3555.83
QVQNYK	–	–	–	–
NQRYFL	–	–	–	–

sequences NLQNYRLLEYK, ADFILVVLSG, KFFEI, and QDLNIFVNYVEIN (Table 2B).

To further examine the amyloid fibril formation propensity of detected peptides, another algorithm, TANGO, was used to calculate their β-sheet aggregation propensity at 25 °C with peptide concentration 0.01 wt%, pH 2 and ionic strength 100 mM (Cheng, et al., 2024; Fernandez-Escamilla, Rousseau, Schymkowitz, & Serrano, 2004). The list of all peptides of FPI fibrils formed by TS-30 or CH-4 treatments and their *AGG* scores is shown in Table S2. Peptides were considered to have high β-sheet propensity if assigned *AGG* scores ≥1 computed by TANGO (Cerda-Costa, Esteras-Chopo, Aviles, Serrano, & Villegas, 2007). As shown in Table S1, in the common 228 peptides generated from TS-30 and CH-4, 166 peptides which had *AGG* scores of ≥1. In addition, there were 29 out of 47 and 44 out of 67 peptides with *AGG* scores of ≥1 in the unique peptides of FPI fibrils formed by TS-30 and CH-4 treatments, respectively. In general, TANGO calculations demonstrated that peptides with a high β-aggregate forming propensity could participate in the formation of amyloid fibrils.

3.5. Characterisation of FPI fibrillar gels

3.5.1. Small and large deformation rheological properties of FPI fibrillar gels

3.5.1.1. Small deformation rheological properties. Gelation and rheological behaviour are among the most critical properties of self-assembled protein fibrils. Understanding the rheological properties of fibrillar gels enables insights to be gained on the relationship between fibril microstructure and their associated macroscopic mechanical properties (Xu et al., 2023). The viscoelastic properties of FPI fibrillar gels as a function of frequency are shown in Fig. 6A. For all the samples, G' and G'' were parallel to each other and only slightly varied with frequency, indicating a prevailing elastic behaviour with a solid-like behaviour in all samples (Banerjee & Bhattacharya, 2012; Wei & Huang, 2020). These results agree well with the observation that self-supporting 10 wt% FPI hydrogels were formed by both TS and CH treatment for 4 h and 8 h (Fig. 1A). Fibrillar gel formation at pH 2 after prolonged heating has been also found in soy protein at 50 g/L after heating from 12 h to 48 h (Xu et al., 2023) and lentil protein at 8 wt% after heating from 4 h to 16 h (Jo, et al., 2020), for examples. This could be due to the formation of a denser and entangled fibril network at pH 2 (Peng, et al., 2018).

To better compare the gel strength, the G' at 1 Hz of all the samples was plotted in Fig. 6C. The CH samples showed greater G' (1 Hz) values compared to the TS samples, indicating that the prolonged CH treatment (4 h and 8 h) was more effective in the formation of the fibrillar gel network with a stronger gel strength, and longer time heating resulting in a stronger gel strength. For instance, G' (1 Hz) increased from ~161 Pa to ~713 Pa when the heat treatment time was increased from 4 h to 8 h. Similar observations have been made in lentil proteins at pH 2 with increasing heating time from 1 to 16 h. It has been suggested that protein molecules could undergo greater unfolding, interactions, and entanglement under longer heating time, thereby forming a stronger gel networks (Jo, et al., 2020). However, the G' (1 Hz) of the TS-induced fibrillar gel (Fig. 6A and C) was lower after 30 min TS (~56 Pa) treatment than TS-20 (~88 Pa), which could be due to a break-down of long FPI fibrils induced by prolonged TS treatment, resulting in a weakened fibril-fibril entanglement and network (Nakajima, et al., 2021; Pathak, Bhangu, Martin, Separovic, & Ashokkumar, 2022). Further, fibrils and other non-fibrillar components including unconverted peptides, soluble and insoluble protein aggregates may co-exist in FPI fibril samples induced by either TS or CH treatment. Depending on their concentrations and assembly state or interactions, their contributions to gel

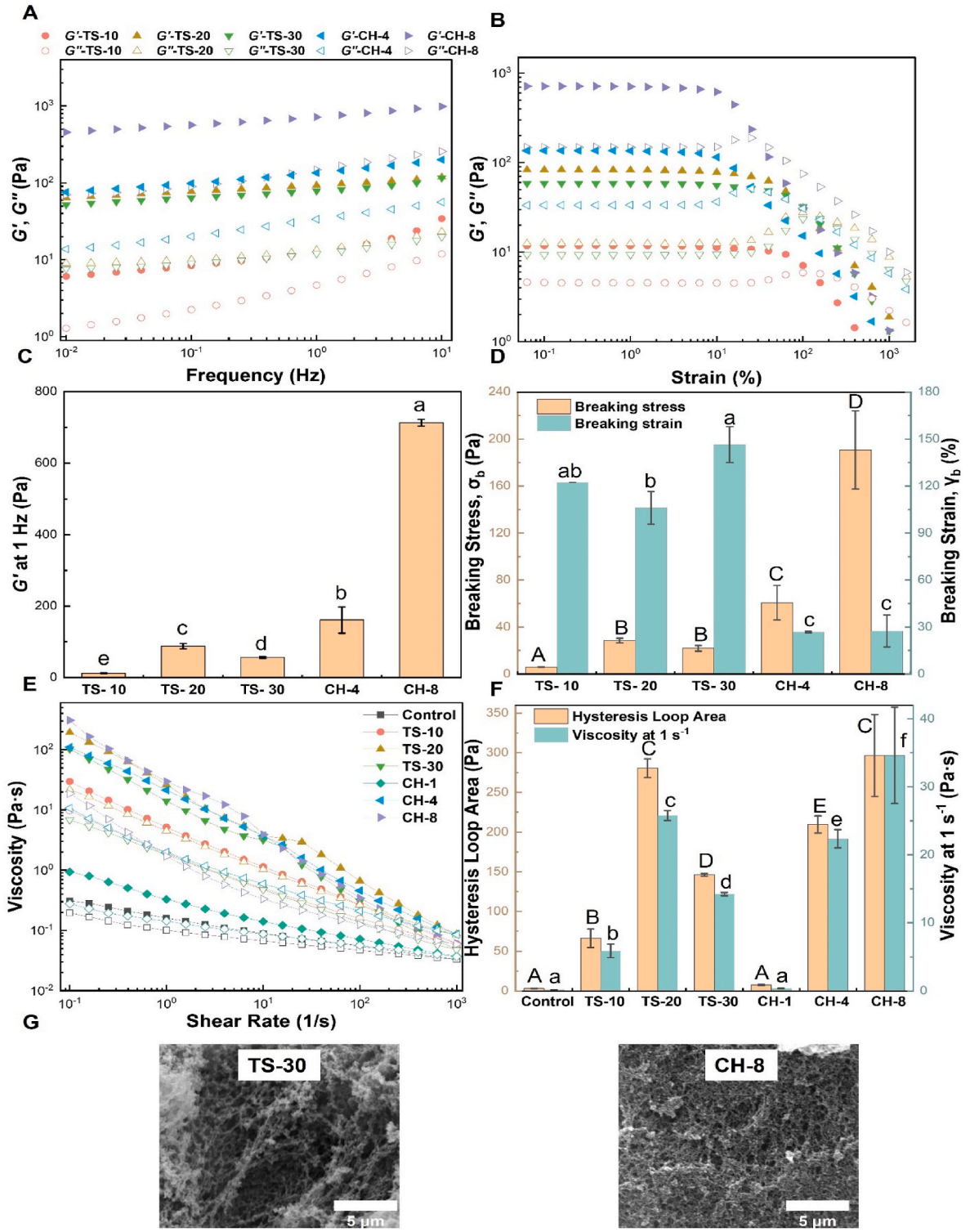

Fig. 6. (A) Storage modulus *G'* (solid symbols) and loss modulus *G''* (empty symbols) as a function of frequency (A) and strain amplitude (B) for faba bean protein isolate (FPI) fibrillar gels induced by different treatment. (C) Gel strength *G'* (1 Hz) (C) and breaking strain (γ_b) and breaking stress (σ_b) (D) for FPI fibrillar gels induced by different treatments. (E) Viscosity as a function of shear rate for FPI fibrils induced by different treatments. Solid and open symbols represent the "up" and "down" measurements, respectively. (F) Thixotropic hysteresis loop area of thermosonciation (TS) and conventional heat treatment (CH) treated FPI fibrils obtained from the "up" and "down" viscosity measurements. (G) SEM images of seleced FPI fibrillar gels (TS-30 and CH-8). In (C, D, and F) different superscript letters above the column denote significant differences ($P < 0.05$).

network formation can be different (Meng, et al., 2022; Yang, de Campo, et al., 2022). This may also lead to different gel strength observed in FPI samples with different treatment and time.

3.5.1.2. Large deformation rheological properties. Large deformation rheological behaviour and structural breakdown characteristics of FPI fibrillar gels were measured by the *strain-sweep* test as shown in Fig. 6B. All samples demonstrated a quantitatively similar strain dependent

behaviour. When the strain amplitude is small, i.e. within the linear viscoelastic region (LVR), both G' and G'' were nearly constant with the increase in strain amplitude. This is a typical characteristic of linear viscoelastic behaviour. In addition, G' was greater than G'' within the LVR, indicating a solid-like structure with a prevailing elastic behaviour as confirmed by the *frequency sweep* measurements and visual appearance (Fig. 1A) (Munialo, Martin, Van Der Linden, & De Jongh, 2014). When the strain amplitude was beyond the LVR, the G' values of all fibrillar gel samples dropped remarkably due to structural disintegration (Yang, de Campo, et al., 2022). On the other hand, for the G'', it firstly increased and reached a maximum before decreasing remarkedly with the strain increase, indicating a typical type III nonlinear rheological (weak strain overshoot) behaviour (Hyun, Kim, Ahn, & Lee, 2002). This could be caused by an increase in flow or energy dissipation induced by structural rearrangement such as disentanglement of the fibril network (Nechyporchuk, Belgacem, & Pignon, 2016; Zhang, Cheng, Luo, Hemar, & Yang, 2021). Similar results were reported in previous large deformation rheological studies on other fibrillar gel systems such as cellulose nanofibril hydrogels (Krüger, et al., 2020) and β-hairpin peptide hydrogels (Micklitsch, et al., 2015). With a further increase in strain amplitude, a crossover of G' and G'' occurred and the corresponding strain and stress at the crossover point ($G' = G''$) were defined as breaking strain and breaking stress, respectively. Beyond this point, G'' is dominant over G', suggesting flow of samples due to significant structural disintegration (Yang, et al., 2016). To further compare large deformation rheological behaviour among different gel samples, the breaking stress (σ_b) and breaking strain (γ_b) of all the samples are shown in Fig. 6D. For CH induced fibrillar gels, the σ_b increased with an increase in treatment time, but σ_b firstly increased when TS treatment time increased from 10 to 20 min and then slightly reduced in the TS-30 sample, following a similar trend to G' at 1 Hz (Fig. 6C). For example, CH-8 exhibited the greatest value of σ_b (~191 Pa) among all samples, while TS-20 had the largest σ_b (~28 Pa) among TS induced FPI fibrillar gel samples.

As shown in Fig. 6D, fibrillar gels induced by TS treatments had much larger γ_b values than their CH counterparts) For example, the γ_b values of TS fibrillar gels were in the range of ~120–150%, while the γ_b values of CH fibrillar gels were much smaller at ~30%. This indicated that the TS fibrillar gels could withstand a significant larger shear deformation before breaking down. It has been suggested that rheological properties of fibrillar gels are closely related to their microstructural characteristics including contour length, flexibility, and aspect ratio of the individual fibrils as well as fibril-fibril entanglement and interactions (Cen, et al., 2022; Rodriguez, Hemar, Cornish, & Brimble, 2016; Xu et al., 2023). These results therefore suggest that different treatments (CH and TS) could result in FPI fibrillar gels with distinct structural characteristics.

3.5.2. *Viscosity of FPI fibrillar gels*

Flow curves of the control, CH- and TS-treated 10 wt% FPI dispersions at different treatment times are shown in Fig. 6E. All samples displayed shear-thinning behaviour in which the viscosity decreases as the shear rate increases. Compared to the control, CH and TS treated FPI samples showed a significant increase in viscosities and stronger shear thinning behaviour, which could be due to formation of a denser network induced by entanglements of the fibrils (Kuijk, et al., 2013; Peng et al., 2018). To better compare viscosities among different samples, values at 1 s^{-1} are plotted as shown in Fig. 6F. It can be observed that the control and CH-1 samples had a significantly lower viscosity compared to other TS and CH samples, which was in line with the visual observation in Fig. 1A. Specifically, TS-20 had the greatest viscosity (~25.8 Pa s) among TS samples, and viscosity significantly increased (from ~0.4 to ~34.6 Pa s) for CH samples with heating time increasing from 1 h to 8 h. Similar shear-thinning behaviour of plant protein fibrillar gels had also been observed in soybean protein fibrils (Ji, et al., 2021) and rice bean protein fibrils (Zhang et al., 2014).

The "up" and "down" viscosity sweep measurements are shown in Fig. 6E. For all samples, the viscosity was lower upon decreasing the shear rate compared to the viscosity when the shear rate was increased. The presence of a hysteresis loop suggests that FPI fibrillar gels were thixotropic with a time-dependent flow behaviour (Peng, et al., 2018). The hysteresis loop area between the up and down curves was calculated to investigate the extent of thixotropy, where the larger area corresponded to stronger thixotropic behaviour and larger protein fibrillar aggregates (Armelin, et al., 2006; Luo et al., 2021). The hysteresis loop areas calculated from all FPI samples are presented in Fig. 6F. The change of hysteresis loop area among samples was in line with the viscosities at 1 s^{-1} (Fig. 6F). The CH-8 sample had a largest hysteresis loop area (~297 Pa) followed by the TS-20 sample (~281Pa). This hysteresis behaviour was also observed for WPI fibrils (Peng, et al., 2018) and wood cellulose microfibrils (De Kort, et al., 2016).

3.5.3. *Microstructural network characteristics of FPI fibrillar gels by SEM*

The microstructures of selected FPI fibrillar gels induced by different methods (TS-30 and CH-8) were observed by SEM (Fig. 6G). For both samples, it can be clearly seen that fine-stranded fibrils are entangled and crosslinked, leading to the formation of network structure with thin connective walls composed of flexible fibrillar aggregates. Similar SEM morphologies of fibrillar gels have been reported for lentil proteins and pea proteins (Jo, et al., 2020; Zhu, Huang, & Chen, 2022). Furthermore, CH-8 samples exhibited a more compact and much denser fibrillar protein network structure than the TS-30 sample. This might explain the greater gel strength and larger extent of thixotropic behaviour in CH-8 gels. This is because the hysteresis area is related to the energy required to disrupt the internal structures within the gels, so it is expected that FPI fibrillar gels with large and compact aggregates required higher energy to destroy the internal structure contributing to a greater hysteresis (Dankar, Haddarah, El Omar, Sepulcre, & Pujolà, 2018; Luo et al., 2021). In contrast, uneven, less compact protein network structures with large porosity was observed in TS-30 fibrillar gel, leading to their weaker gel strength as discussed above.

3.5.4. *Thermo-reversible gelation of FPI fibrillar gels*

A study on rheological response of hydrogels to environmental factors such as temperature is important for their application and also to help understand the underlying gelation mechanism (De Kort, et al., 2016; Yang, Yang, & Yang, 2018). Therefore, the rheological properties of TS-30 fibrillar gel as a function of temperature were studied. Fig. 7

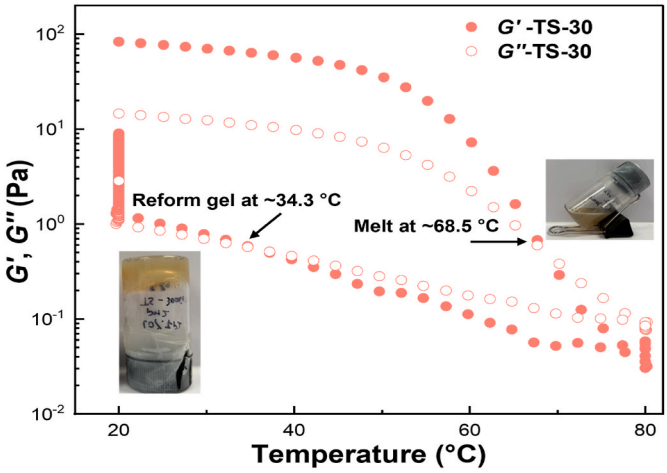

Fig. 7. Storage modulus G' (solid symbols) and loss modulus G'' (empty symbols) as a function of temperature for faba bean protein isolate (FPI) sample treated by thermosonciation for 30 min (TS-30) during a rheological temperature sweep measurement (*inset*: visual appreance of samples during sol-gel and gel-sol transitions).

andFig. S2 show G' and G'' of TS-30 fibrillar gel as a function of temperature and time, respectively. As the temperature increased from 20 to ~60 °C, G' and G'' gradually decreased but G' was still larger than G'', indicating the sample was still in the solid state. When the temperature was further increased from 60 to 80 °C, both G' and G'' decreased considerably and G' decreased much faster than G''; this resulted in a crossover of G' and G'' at ~68.5 °C. This temperature can be defined as the melting temperature and beyond this temperature G'' was larger than G', suggesting a gel to solution transition had occurred and the sample was flowable (Fig. 7 inset). Upon cooling, both G' and G'' increased progressively with G' increasing faster than G''. Therefore, at a certain temperature (~34.3 °C), $G' = G''$ was reached and below this temperature G' was larger than G'' suggesting the liquid like sample solidified again to form self-supporting hydrogel (Fig. 7 inset). The FPI solution was re-gelled during cooling, and a gradual increase in G' was observed when temperature was maintained at 20 °C for 2 h, indicating that the gel network was formed during the cooling process. Based on this result, it can be inferred that hydrogen bonding is critical in formation of the fibrillar gel network where hydrogen bonding is reinforced at a low temperature while being diminished at a high temperature (Cen, et al., 2023; Damodaran, 2008; Yang, de Campo, et al., 2022). To the best of our knowledge, reports on thermally reversible gels derived from plant proteins are scant. Recently, Zhu et al. (2022) developed thermally reversible pea protein gels, however, pea proteins need to be extracted by using an ammonium sulfate precipitation method. Our study suggests that the thermally reversible FPI gel can be simply made using TS treatment, and the gel may have the potential to substitute gelatine in vegan products.

3.6. Physicochemical properties and microstructural characteristics of HIPEs made from FPI fibrils

3.6.1. Oil-water interfacial tension

The interfacial tension (IFT) of FPI dispersions before and after TS-30 treatment at pH 2 as a function of time is shown in Fig. 8A. The interfacial tension of both samples initially decreased remarkably with time and tended to reach an equilibrium at ~5000 s, which is a typical behaviour of proteins suggesting that proteins have adopted their stable conformations after migrating from the aqueous phase to the oil-water interface (Tang, 2020). The IFT values at 5000 s are shown in Fig. 8A inset and were ~15.8 mN/m (control) and to ~14.0 mN/m for the TS-30 sample. This finding indicated that TS-30 FPI fibrils are more surface active and capable of reducing the oil-water interfacial tension, in line with previous outcomes of SPI fibrils (Ansarifar, et al., 2019). This may be due to the high aspect ratio of protein fibrils and/or the presence of surface-active peptides resulting from protein hydrolysis (Xu et al., 2023).

3.6.2. Oil droplet sizes distributions of HIPEs

The droplet size distributions of HIPEs ($\varphi = 75\%$) stabilised by native FPI dispersion (E-control) or TS-30 FPI fibrils (3 wt%, pH 2) (E-TS-30) are shown in Fig. 8B. The droplet size distributions of E-Control and E-TS-30 were different, where E-Control had a prominent peak at ~30 μm, but E-TS-30 had a much smaller size with a prominent peak around 20 μm. Furthermore, the D [3,2] of E-TS-30 (~17.6 μm) was much smaller than that of E-control (~21.2 μm) (Fig. 8B, inset). This finding was in agreement with the interfacial tension results (Fig. 8A), that the superior emulsification capability of TS-30 FPI fibrils could stabilise larger surface areas leading to smaller oil droplet size. Similar findings were reported in previous studies (e.g., β-lactoglobulin and lentil protein isolate) (Gao, et al., 2017; Wynnychuk, Jo, Chu, & Chen, 2021). For example, Wynnychuk et al. (2021) studied the O/W emulsions (φ = 50%) stabilised by 1.5 wt% lentil protein fibrils induced by conventional heat treatment under pH 2 at 90 °C for 2 h. The results showed that the oil droplet size (D_{90}) of emulsions stabilised by fibrils was smaller (~35 μm) compared to emulsions stabilised by unheated proteins (~45 μm).

3.6.3. Microstructure of HIPEs as influenced by FPI structures

CLSM was employed to examine the microstructural characteristics of the HIPEs stabilised by 3 wt% FPI and TS-30 FPI fibrils at pH 2, and the micrographs are shown in Fig. 8C. Oil droplets stained by Nile Red are shown in red while the protein stained by Fast Green is shown in green. For both emulsion samples, oil droplets were closely packed, and compressed, demonstrating a typical structural characteristics of HIPEs (Zhang, Cheng, et al., 2021; Zhang et al., 2021). Additionally, it can be observed that the oil droplet size decreased when the emulsions are stabilised by TS-30 fibrils compared to native FPI proteins, which was in line with oil droplet size distribution results (Fig. 8B). Moreover, in the E-TS-30 sample, oil droplets were more compact and more densely packed, showing polyhedron type shapes. Similar microstructural characteristics were also observed in pea protein fibril (2 wt%, formed by heating at 85 °C, 20 h at pH 2) stabilised HIPEs with oil fractions of 80% (Wu, Nian, Liu, Zhang, & Hu, 2022).

3.6.4. Rheological properties of HIPEs

The G' and G'' of the HIPEs stabilised by control or TS-30 fibrils as a function of frequency are showed in Fig. 8D. For both emulsion samples, G' and G'' were nearly independent of frequency with G' being greater more than ten times greater G'', indicating strong gel and solid-like characteristics dominated by elasticity (Hu, et al., 2023). This agrees well with the visual appearance (Fig. 8D inset) that both FPI stabilised emulsions formed strong and self-supporting gels that can adhere to the bottom of the vial after inversion. The solid and gel-like characteristics of HIPEs have been widely reported in HIPEs stabilised by plant proteins such as quinoa protein isolate (Zhang, Cheng, et al., 2021) and pea protein isolate (Wu, et al., 2022). This has been attributed to the densely packed oil droplets as observed by CLSM (Fig. 8C and D). In addition, the TS-30 FPI fibril stabilised HIPEs demonstrated a stronger gel network than native FPI (control) stabilised HIPEs. Specifically, the E-TS-30 sample had a greater G' (1 Hz) (~950 Pa) than E-control (~600 Pa). The more compact and tightly arranged oil droplets of smaller size with a possible protein fibril network in the aqueous phase could lead to stronger resistance of oil droplets against movement, thus resulting in a greater mechanical strength of HIPE stabilised by TS-30 FPI fibrils of E-TS-30 (Wei, Cheng, & Huang, 2019). Similar observations have been made in O/W HIPEs ($\varphi = 0.8$) stabilised by WPI and WPI fibrils. It has been reported that WPI fibrils stabilised HIPEs had a greater G' and hardness than WPI stabilised HIPEs (Yang, Jiao, et al., 2022). In addition, the presence of non-fibrillar components such as unconverted peptides and soluble protein aggregates in FPI fibril samples may also play important roles in stabilising HIPEs and contributing to a stronger gel strength (Gao, et al., 2017; Mantovani et al., 2018).

Large deformation rheological behaviour and structural breakdown characteristics of emulsions are shown in Fig. 8E and G. Within the LVR, G' was greater than G'' and both HIPEs were independent of the applied strain amplitude. As the strain amplitude was beyond the LVR, G' and G'' decreased significantly indicating the structure of HPIEs started to breakdown. Also, a clear overshoot of G'' was observed when the strain was close to the crossover point (i.e., type III nonlinear behaviour) (Hyun, et al., 2002). This behaviour has been reported on HIPEs stabilised by quinoa protein isolate (Zhang, Cheng, et al., 2021), which was attributed to energy dissipation caused by structural rearrangement under large strain deformation (Masalova, Foudazi, & Malkin, 2011; Mason, Bibette, & Weitz, 1995; Zhang, Cheng, et al., 2021). With a further increase in strain amplitude, the inter-oil droplet interactions were destroyed, leading to the occurrence of G' and G'' crossover. The corresponding strain and stress at the crossover point were defined as breaking strain and breaking stress, respectively as shown in Fig. 8G. It was found that the breaking stress of E-TS-30 was significantly greater (~180 Pa) than that of E-Control (~120 Pa), which agrees well with the small oscillatory deformation results. However, the breaking strain is similar for both samples (~35%). Beyond the crossover point, G'' became higher than G', implying that the gel structure was significantly

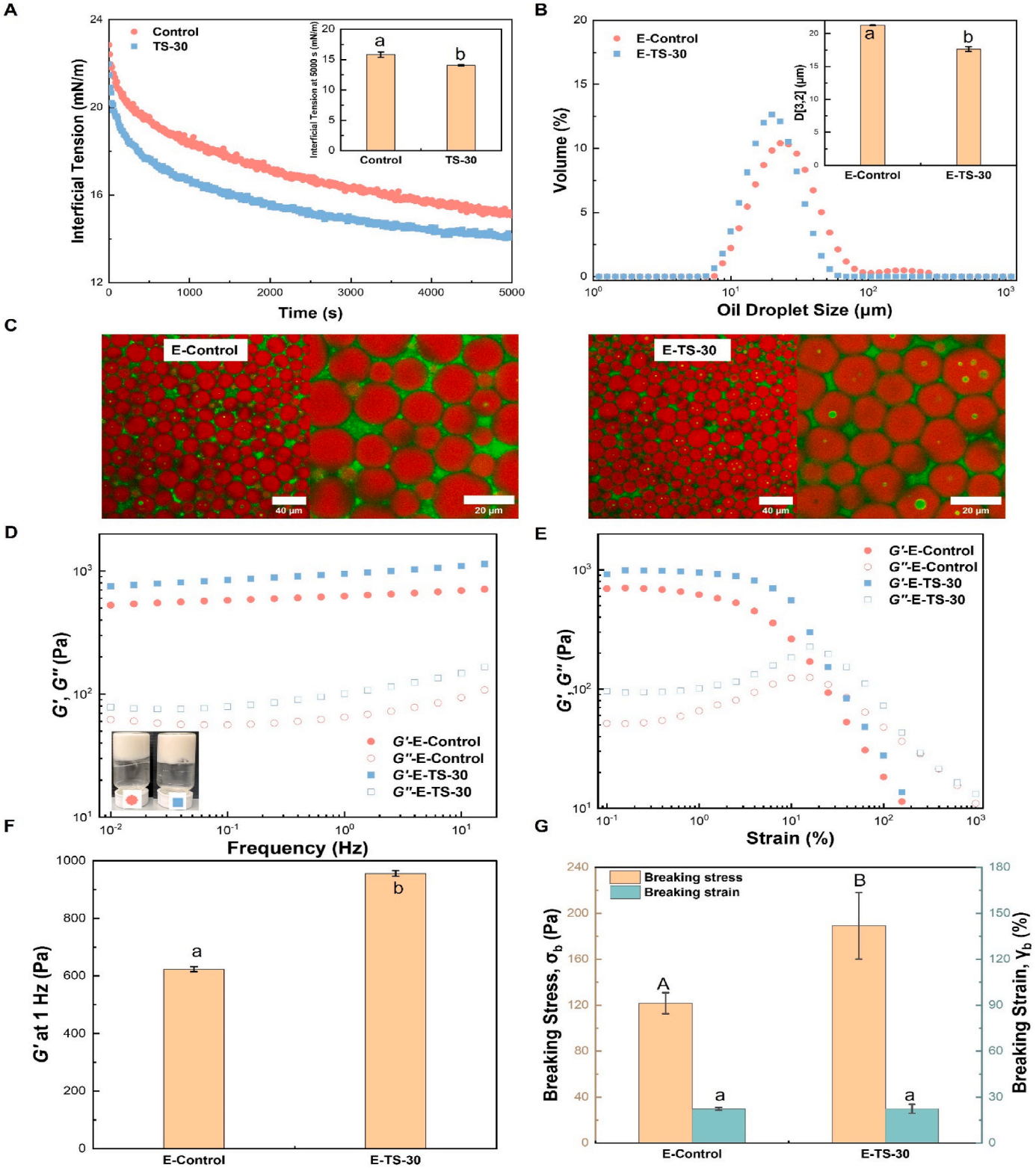

Fig. 8. (A) Oil-water interfacial tension of faba bean protein isolate (FPI) before and after 30 min thermosonication treatment (TS-30), and final interfacial tension values at 5000 s (*inset*). (B) Oil droplet size distribution of HIPEs stabilised by 3 wt% native FPI solution and FPI fibrils (TS-30). Insets are Sauter mean diameter D [3,2] of oil droplets. (C) Confocal micrographs of HIPEs stabilised by 3 wt% native FPI solution and FPI fibrils (TS-30). Scale bar is 40 μm. Insets associated zoom-in images with scale bar of 20 μm. (D) The frequency dependence of G' (solid symbols) and G'' (empty symbols) for HIPEs stabilised by native FPI and FPI fibrils (TS-30). Insets are visual appearance of HIPEs. (E) The strain amplitude dependence of G' (solid symbols) and G'' (emptysymbols) for HIPEs stabilised by native FPI and FPI fibrils (TS-30). (F) Gel strength G' (1 Hz) and breaking strain (γ_b) and breaking stress (σ_b) for HIPEs stabilised by native FPI and FPI fibrils (TS-30). In (A, B, F, and G) different superscript letters above the column, denote significant differences ($P < 0.05$). E-control and E-TS-30 indicate the HIPEs stabilised by native FPI and FPI fibrils (TS-30), respectively.

destroyed and started to flow.

4. Conclusions

This study systematically compared two methods including thermosonication (TS) and conventional heating (CH) on the fibrillisation of faba bean protein isolates (FPI) at pH 2. The results demonstrated that although both methods could successfully form amyloid fibrils with a high aspect ratio and dominated by β-sheet secondary structures, TS could significantly accelerate the fibril formation. This could be due to the high solubility and more extensive degradation of FPI when exposed to ultrasonication at elevated temperatures, thus promoting fibril self-assembly during cooling. The building blocks of FPI fibrils were characterised by LC-MS/MS and there were 47 and 67 unique peptides identified from TS-30 and CH-4 treatment, respectively. A few peptide sequences such as GFSSEFLAQTFNTEEDTAKR from legumin and ADFILVVLSGK from vicilin were identified as amyloidogenic core regions for fibril formations according to WALTZ. Formation of amyloid-like fibrils was also evidenced by an increase in ThT fluorescence intensity, a higher content of β-sheet secondary structure, and fibrous nanoscale morphology within an entangled network as revealed by TEM and SANS. Increases in viscosity and the formation of a viscoelastic network were observed in 10 wt% FPI fibril solutions, indicating their potential applications in tuning rheological properties of food. Finally, the TS-induced FPI fibrils were used to stabilise HIPEs ($\varphi = 75\%$), and the HIPEs formed by TS-30 had microstructural features with smaller oil droplet size, greater mechanical strength, and more compact packed oil droplets than HIPEs formed by untreated proteins. This study showed the TS treatment was effective in the preparing of plant protein fibrils. The resultant formed fibrils provide a range of potential applications including as gelling and emulsifying agents.

CRediT authorship contribution statement

Yinxuan Hu: Writing – original draft, Visualization, Software, Methodology, Investigation, Formal analysis, Data curation. **Lirong Cheng:** Writing – review & editing, Validation, Supervision, Formal analysis, Data curation. **Elliot Paul Gilbert:** Writing – review & editing, Visualization, Validation, Software, Resources, Methodology, Investigation, Formal analysis, Data curation. **Trevor S. Loo:** Writing – review & editing, Software, Resources, Methodology, Formal analysis, Data curation. **Sung Je Lee:** Writing – review & editing, Validation, Supervision. **John Harrison:** Writing – review & editing, Validation, Supervision, Software, Resources. **Zhi Yang:** Writing – review & editing, Writing – original draft, Visualization, Validation, Supervision, Software, Resources, Project administration, Methodology, Funding acquisition, Formal analysis, Data curation, Conceptualization.

Declaration of competing interest

The authors declare that they do not have conflict of interest.

Data availability

Data will be made available on request.

Acknowledgements

The author Yinxuan Hu thanks the Massey University, New Zealand for a doctoral student scholarship. We also thank the Manawatu Microscopy and Imaging Centre at Massey University, Palmerston North for technical support.

Appendix A. Supplementary data

Supplementary data to this article can be found online at https://doi.org/10.1016/j.foodhyd.2024.110127.

References

Aggeli, A., Nyrkova, I. A., Bell, M., Harding, R., Carrick, L., McLeish, T. C., et al. (2001). Hierarchical self-assembly of chiral rod-like molecules as a model for peptide β-sheet tapes, ribbons, fibrils, and fibers. *Proceedings of the National Academy of Sciences, 98*(21), 11857–11862.

Akkermans, C., Van der Goot, A., Venema, P., Gruppen, H., Vereijken, J., Van der Linden, E., et al. (2007). Micrometer-sized fibrillar protein aggregates from soy glycinin and soy protein isolate. *Journal of Agricultural and Food Chemistry, 55*(24), 9877–9882.

Alavi, F., Chen, L., & Emam-Djomeh, Z. (2021a). Effect of ultrasound-assisted alkaline treatment on functional property modifications of faba bean protein. *Food Chemistry, 354*, Article 129494.

Alavi, F., Chen, L., Wang, Z., & Emam-Djomeh, Z. (2021b). Consequences of heating under alkaline pH alone or in the presence of maltodextrin on solubility, emulsifying and foaming properties of faba bean protein. *Food Hydrocolloids, 112*, Article 106335.

Alavi, F., Emam-Djomeh, Z., Mohammadian, M., Salami, M., & Moosavi-Movahedi, A. A. (2020). Physico-chemical and foaming properties of nanofibrillated egg white protein and its functionality in meringue batter. *Food Hydrocolloids, 101*, Article 105554.

Ansarifar, E., Shahidi, F., Mohebbi, M., Ramezanian, N., Koocheki, A., & Mohamadian, A. (2019). Optimization of limonene microencapsulation based on native and fibril soy protein isolate by VIKOR method. *Lebensmittel-Wissenschaft und -Technologie, 115*, Article 107884.

Armelin, E., Martí, M., Rudé, E., Labanda, J., Llorens, J., & Alemán, C. (2006). A simple model to describe the thixotropic behavior of paints. *Progress in Organic Coatings, 57*(3), 229–235.

Arrondo, J. L. R., Muga, A., Castresana, J., & Goñi, F. M. (1993). Quantitative studies of the structure of proteins in solution by Fourier-transform infrared spectroscopy. *Progress in Biophysics and Molecular Biology, 59*(1), 23–56.

Banerjee, S., & Bhattacharya, S. (2012). Food gels: Gelling process and new applications. *Critical Reviews in Food Science and Nutrition, 52*(4), 334–346.

Biancalana, M., & Koide, S. (2010). Molecular mechanism of Thioflavin-T binding to amyloid fibrils. *Biochimica et Biophysica Acta (BBA) - Proteins & Proteomics, 1804*(7), 1405–1412.

Bolder, S. G., Hendrickx, H., Sagis, L. M., & Van der Linden, E. (2006). Ca2+-induced cold-set gelation of whey protein isolate fibrils. *Applied Rheology, 16*(5), 258–264.

Bolder, S. G., Sagis, L. M., Venema, P., & van der Linden, E. (2007). Thioflavin T and birefringence assays to determine the conversion of proteins into fibrils. *Langmuir, 23*(8), 4144–4147.

Cao, Y., & Mezzenga, R. (2019). Food protein amyloid fibrils: Origin, structure, formation, characterization, applications and health implications. *Advances in Colloid and Interface Science, 269*, 334–356.

Cen, K., Huang, C., Yu, X., Gao, C., Yang, Y., Tang, X., et al. (2023). Quinoa protein pickering emulsion: A promising cryoprotectant to enhance the freeze-thaw stability of fish myofibril gels. *Food Chemistry, 407*, Article 135139.

Cen, K., Yu, X., Gao, C., Yang, Y., Tang, X., & Feng, X. (2022). Effects of quinoa protein Pickering emulsion on the properties, structure and intermolecular interactions of myofibrillar protein gel. *Food Chemistry, 394*, Article 133456.

Cerda-Costa, N., Esteras-Chopo, A., Aviles, F., Serrano, L., & Villegas, V. (2007). Early kinetics of amyloid fibril formation reveals conformational reorganisation of initial aggregates. *Journal of Molecular Biology, 366*(4), 1351–1363.

Chatani, E., Lee, Y.-H., Yagi, H., Yoshimura, Y., Naiki, H., & Goto, Y. (2009). Ultrasonication-dependent production and breakdown lead to minimum-sized amyloid fibrils. *Proceedings of the National Academy of Sciences, 106*(27), 11119–11124.

Chen, D., Fang, F., Federici, E., Campanella, O., & Jones, O. G. (2020). Rheology, microstructure and phase behavior of potato starch-protein fibril mixed gel. *Carbohydrate Polymers, 239*, Article 116247.

Chen, S., Goode, A. E., Skepper, J. N., Thorley, A. J., Seiffert, J. M., Chung, K. F., et al. (2016). Avoiding artefacts during electron microscopy of silver nanomaterials exposed to biological environments. *Journal of Microscopy, 261*(2), 157–166.

Cheng, L., De Leon-Rodriguez, L. M., Gilbert, E. P., Loo, T., Petters, L., & Yang, Z. (2024). Self-assembly and hydrogelation of a potential bioactive peptide derived from quinoa proteins. *International Journal of Biological Macromolecules, 259*, Article 129296.

Contamine, R. F., Wilhelm, A., Berlan, J., & Delmas, H. (1995). Power measurement in sonochemistry. *Ultrasonics Sonochemistry, 2*(1), S43–S47.

da Silva, A. M. M., Almeida, F. S., & Sato, A. C. K. (2021). Functional characterization of commercial plant proteins and their application on stabilization of emulsions. *Journal of Food Engineering, 292*, Article 110277.

Damodaran, S. (2008). Amino acids, peptides and proteins. *Fennema's Food Chemistry, 4*, 425–439.

Dankar, I., Haddarah, A., El Omar, F., Sepulcre, F., & Pujolà, M. (2018). Assessing the microstructural and rheological changes induced by food additives on potato puree. *Food Chemistry, 240*, 304–313.

De Kort, D. W., Veen, S. J., Van As, H., Bonn, D., Velikov, K. P., & Van Duynhoven, J. P. (2016). Yielding and flow of cellulose microfibril dispersions in the presence of a charged polymer. *Soft Matter, 12*(21), 4739–4744.

de la Rosa-Millán, J., Orona-Padilla, J. L., Flores-Moreno, V. M., & Serna-Saldívar, S. O. (2018). Physicochemical, functional and ATR-FTIR molecular analysis of protein

extracts derived from starchy pulses. *International Journal of Food Science and Technology, 53*(6), 1414–1424.
Dhull, S. B., Kidwai, M. K., Noor, R., Chawla, P., & Rose, P. K. (2022). A review of nutritional profile and processing of faba bean (*Vicia faba* L.). *Legume Science, 4*(3), Article e129.
Fernandez-Escamilla, A.-M., Rousseau, F., Schymkowitz, J., & Serrano, L. (2004). Prediction of sequence-dependent and mutational effects on the aggregation of peptides and proteins. *Nature Biotechnology, 22*(10), 1302–1306.
Frydenberg, R. P., Hammershøj, M., Andersen, U., Greve, M. T., & Wiking, L. (2016). Protein denaturation of whey protein isolates (WPIs) induced by high intensity ultrasound during heat gelation. *Food Chemistry, 192*, 415–423.
Gao, Z., Zhao, J., Huang, Y., Yao, X., Zhang, K., Fang, Y., et al. (2017). Edible Pickering emulsion stabilized by protein fibrils. Part 1: Effects of pH and fibrils concentration. *Lebensmittel-Wissenschaft & Technologie, 76*, 1–8.
Gharibzahedi, S. M. T., & Smith, B. (2020). The functional modification of legume proteins by ultrasonication: A review. *Trends in Food Science & Technology, 98*, 107–116.
Gilbert, E. P., Schulz, J. C., & Noakes, T. J. (2006). 'Quokka'—the small-angle neutron scattering instrument at OPAL. *Physica B: Condensed Matter, 385*, 1180–1182.
Goeden-Wood, N. L., Keasling, J. D., & Muller, S. J. (2003). Self-assembly of a designed protein polymer into β-sheet fibrils and responsive gels. *Macromolecules, 36*(8), 2932–2938.
Greenfield, N. J. (2006). Using circular dichroism spectra to estimate protein secondary structure. *Nature Protocols, 1*(6), 2876–2890.
Guinier, A., Fournet, G., Walker, C. B., & Yudowitch, K. L. (1955). *Small-angle scattering of X-rays*. New York: Wiley.
Herneke, A., Lendel, C., Johansson, D., Newson, W., Hedenqvist, M., Karkehabadi, S., et al. (2021). Protein nanofibrils for sustainable food–characterization and comparison of fibrils from a broad range of plant protein isolates. *ACS Food Science & Technology, 1*(5), 854–864.
Herneke, A., Lendel, C., Karkehabadi, S., Lu, J., & Langton, M. (2023). Protein nanofibrils from fava bean and its major storage proteins: Formation and ability to generate and stabilise foams. *Foods, 12*(3), 521.
Hettiarachchi, C. A., Melton, L. D., Gerrard, J. A., & Loveday, S. M. (2012). Formation of β-lactoglobulin nanofibrils by microwave heating gives a peptide composition different from conventional heating. *Biomacromolecules, 13*(9), 2868–2880.
Hong, D.-P., Han, S., L Fink, A., & N Uversky, V. (2011). Characterization of the non-fibrillar α-synuclein oligomers. *Protein and Peptide Letters, 18*(3), 230–240.
Hu, Y., Cheng, L., Lee, S. J., & Yang, Z. (2023). Formation and characterisation of concentrated emulsion gels stabilised by faba bean protein isolate and its applications for 3D food printing. *Colloids and Surfaces A: Physicochemical and Engineering Aspects*, Article 131622.
Hu, Y., He, C., Woo, M. W., Xiong, H., Hu, J., & Zhao, Q. (2019). Formation of fibrils derived from whey protein isolate: Structural characteristics and protease resistance. *Food & Function, 10*(12), 8106–8115.
Hu, A., & Li, L. (2021). Effect mechanism of ultrasound pretreatment on fibrillation Kinetics, physicochemical properties and structure characteristics of soy protein isolate nanofibrils. *Ultrasonics Sonochemistry, 78*, Article 105741.
Husband, F., Wilde, P., Clark, D., Rawel, H., & Muschiolik, G. (1994). Foaming properties of modified faba bean protein isolates. *Food Hydrocolloids, 8*(5), 455–468.
Hyun, K., Kim, S. H., Ahn, K. H., & Lee, S. J. (2002). Large amplitude oscillatory shear as a way to classify the complex fluids. *Journal of Non-newtonian Fluid Mechanics, 107*(1–3), 51–65.
Ji, F., Xu, J., Ouyang, Y., Mu, D., Li, X., Luo, S., et al. (2021). Effects of NaCl concentration and temperature on fibrillation, structure, and functional properties of soy protein isolate fibril dispersions. *Lebensmittel-Wissenschaft & Technologie, 149*, Article 111862.
Jo, Y.-J., Huang, W., & Chen, L. (2020). Fabrication and characterization of lentil protein gels from fibrillar aggregates and the gelling mechanism study. *Food & Function, 11*(11), 10114–10125.
Josefsson, L., Ye, X., Brett, C. J., Meijer, J., Olsson, C., Sjögren, A., et al. (2019). Potato protein nanofibrils produced from a starch industry sidestream. *ACS Sustainable Chemistry & Engineering, 8*(2), 1058–1067.
Kamada, A., Rodriguez-Garcia, M., Ruggeri, F. S., Shen, Y., Levin, A., & Knowles, T. P. (2021). Controlled self-assembly of plant proteins into high-performance multifunctional nanostructured films. *Nature Communications, 12*(1), 3529.
Kline, S. R. (2006). Reduction and analysis of SANS and USANS data using IGOR Pro. *Journal of Applied Crystallography, 39*(6), 895–900.
Krüger, M., Oosterhoff, L. A., van Wolferen, M. E., Schiele, S. A., Walther, A., Geijsen, N., et al. (2020). Cellulose nanofibril hydrogel promotes hepatic differentiation of human liver organoids. *Advanced Healthcare Materials, 9*(6), Article 1901658.
Kuijk, A., Koppert, R., Versluis, P., van Dalen, G., Remijn, C., Hazekamp, J., et al. (2013). Dispersions of attractive semiflexible fiberlike colloidal particles from bacterial cellulose microfibrils. *Langmuir, 29*(47), 14356–14360.
Kutzli, I., Zhou, J., Li, T., Baier, S. K., & Mezzenga, R. (2023). Formation and characterization of plant-based amyloid fibrils from hemp seed protein. *Food Hydrocolloids, 137*, Article 108307.
Laemmli, U. K. (1970). Cleavage of structural proteins during the assembly of the head of bacteriophage T4. *Nature, 227*(5259), 680–685.
Lattanzi, V., André, I., Gasser, U., Dubackic, M., Olsson, U., & Linse, S. (2021). Amyloid β 42 fibril structure based on small-angle scattering. *Proceedings of the National Academy of Sciences, 118*(48), Article e2112783118.
Li, T., Wang, L., Geng, H., Zhang, X., & Chen, Z. (2021a). Formation, structural characteristics, foaming and emulsifying properties of rice glutelin fibrils. *Food Chemistry, 354*, Article 129554.
Li, T., Wang, L., Zhang, X., Geng, H., Xue, W., & Chen, Z. (2021b). Assembly behavior, structural characterization and rheological properties of legume proteins based amyloid fibrils. *Food Hydrocolloids, 111*, Article 106396.
Li, T., Zhou, J., Peydayesh, M., Yao, Y., Bagnani, M., Kutzli, I., et al. (2023a). Plant protein amyloid fibrils for multifunctional sustainable materials. *Advanced Sustainable Systems, 7*(4), Article 2200414.
Li, T., Zhou, J., Wu, Q., Zhang, X., Chen, Z., & Wang, L. (2023b). Modifying functional properties of food amyloid-based nanostructures from rice glutelin. *Food Chemistry, 398*, Article 133798.
Liu, Q., Yang, Q., Wang, Y., Jiang, Y., & Chen, H. (2023). Formation and structural characteristics of pea globulin amyloid-like fibrils pretreated with low-frequency magnetic field. *Food Hydrocolloids, 109331*.
Luo, L., Yang, Z., Wang, H., Ashokkumar, M., & Hemar, Y. (2022). Impacts of sonication and high hydrostatic pressure on the structural and physicochemical properties of quinoa protein isolate dispersions at acidic, neutral and alkaline pHs. *Ultrasonics Sonochemistry, 91*, Article 106232.
Luo, L., Zhang, R., Palmer, J., Hemar, Y., & Yang, Z. (2021). Impact of high hydrostatic pressure on the gelation behavior and microstructure of quinoa protein isolate dispersions. *ACS Food Science & Technology, 1*(11), 2144–2151.
Mantovani, R. A., de Figueiredo Furtado, G., Netto, F. M., & Cunha, R. L. (2018). Assessing the potential of whey protein fibril as emulsifier. *Journal of Food Engineering, 223*, 99–108.
Martínez-Velasco, A., Lobato-Calleros, C., Hernández-Rodríguez, B. E., Román-Guerrero, A., Alvarez-Ramirez, J., & Vernon-Carter, E. J. (2018). High intensity ultrasound treatment of faba bean (*Vicia faba* L.) protein: Effect on surface properties, foaming ability and structural changes. *Ultrasonics Sonochemistry, 44*, 97–105.
Masalova, I., Foudazi, R., & Malkin, A. Y. (2011). The rheology of highly concentrated emulsions stabilized with different surfactants. *Colloids and Surfaces A: Physicochemical and Engineering Aspects, 375*(1–3), 76–86.
Mason, T., Bibette, J., & Weitz, D. (1995). Elasticity of compressed emulsions. *Physical Review Letters, 75*(10), 2051.
Mason, T. O., Chirgadze, D. Y., Levin, A., Adler-Abramovich, L., Gazit, E., Knowles, T. P., et al. (2014). Expanding the solvent chemical space for self-assembly of dipeptide nanostructures. *ACS Nano, 8*(2), 1243–1253.
Maurer-Stroh, S., Debulpaep, M., Kuemmerer, N., De La Paz, M. L., Martins, I. C., Reumers, J., et al. (2010). Exploring the sequence determinants of amyloid structure using position-specific scoring matrices. *Nature Methods, 7*(3), 237–242.
Meng, Y., Wei, Z., & Xue, C. (2022). Protein fibrils from different food sources: A review of fibrillation conditions, properties, applications and research trends. *Trends in Food Science & Technology, 121*, 59–75.
Micklitsch, C. M., Medina, S. H., Yucel, T., Nagy-Smith, K. J., Pochan, D. J., & Schneider, J. P. (2015). Influence of hydrophobic face amino acids on the hydrogelation of β-hairpin peptide amphiphiles. *Macromolecules, 48*(5), 1281–1288.
Mihara, H., Matsumura, S., & Takahashi, T. (2005). Construction and control of self-assembly of amyloid and fibrous peptides. *Bulletin of the Chemical Society of Japan, 78*(4), 572–590.
Munialo, C. D., Martin, A. H., Van Der Linden, E., & De Jongh, H. H. (2014). Fibril formation from pea protein and subsequent gel formation. *Journal of Agricultural and Food Chemistry, 62*(11), 2418–2427.
Nakajima, K., Nishioka, D., Hirao, M., So, M., Goto, Y., & Ogi, H. (2017). Drastic acceleration of fibrillation of insulin by transient cavitation bubble. *Ultrasonics Sonochemistry, 36*, 206–211.
Nakajima, K., Toda, H., Yamaguchi, K., So, M., Ikenaka, K., Mochizuki, H., et al. (2021). Half-time heat map reveals ultrasonic effects on morphology and kinetics of amyloidogenic aggregation reaction. *ACS Chemical Neuroscience, 12*(18), 3456–3466.
Nasrabadi, M. N., Doost, A. S., & Mezzenga, R. (2021). Modification approaches of plant-based proteins to improve their techno-functionality and use in food products. *Food Hydrocolloids, 118*, Article 106789.
Nechyporchuk, O., Belgacem, M. N., & Pignon, F. (2016). Current progress in rheology of cellulose nanofibril suspensions. *Biomacromolecules, 17*(7), 2311–2320.
Nilsson, M. R. (2004). Techniques to study amyloid fibril formation in vitro. *Methods, 34*(1), 151–160.
Ohhashi, Y., Kihara, M., Naiki, H., & Goto, Y. (2005). Ultrasonication-induced amyloid fibril formation of β2-microglobulin. *Journal of Biological Chemistry, 280*(38), 32843–32848.
Pathak, R., Bhangu, S. K., Martin, G. J., Separovic, F., & Ashokkumar, M. (2022). Ultrasound-induced protein restructuring and ordered aggregation to form amyloid crystals. *European Biophysics Journal, 51*(4–5), 335–352.
Peng, J., Calabrese, V., Veen, S. J., Versluis, P., Velikov, K. P., Venema, P., et al. (2018). Rheology and microstructure of dispersions of protein fibrils and cellulose microfibrils. *Food Hydrocolloids, 82*, 196–208.
Pogostin, B. H., Linse, S., & Olsson, U. (2019). Fibril charge affects α-synuclein hydrogel rheological properties. *Langmuir, 35*(50), 16536–16544.
Rahman, M. M., Hojilla-Evangelista, M. P., & Lamsal, B. P. (2022). Impact of high-power sonication on yield, molecular structure, and functional properties of soy protein isolate. *Innovative Food Science & Emerging Technologies, 79*, Article 103034.
Rodriguez, L. M. D. L., Hemar, Y., Cornish, J., & Brimble, M. A. (2016). Structure–mechanical property correlations of hydrogel forming β-sheet peptides. *Chemical Society Reviews, 45*(17), 4797–4824.
Rubinov, B., Wagner, N., Matmor, M., Regev, O., Ashkenasy, N., & Ashkenasy, G. (2012). Transient fibril structures facilitating nonenzymatic self-replication. *ACS Nano, 6*(9), 7893–7901.

So, M., Yagi, H., Sakurai, K., Ogi, H., Naiki, H., & Goto, Y. (2011). Ultrasonication-dependent acceleration of amyloid fibril formation. *Journal of Molecular Biology, 412*(4), 568–577.

Stanley, C. B., Perevozchikova, T., & Berthelier, V. (2011). Structural formation of huntingtin exon 1 aggregates probed by small-angle neutron scattering. *Biophysical Journal, 100*(10), 2504–2512.

Stathopulos, P. B., Scholz, G. A., Hwang, Y. M., Rumfeldt, J. A., Lepock, J. R., & Meiering, E. M. (2004). Sonication of proteins causes formation of aggregates that resemble amyloid. *Protein Science, 13*(11), 3017–3027.

Sun, C., Wang, C., Xiong, Z., & Fang, Y. (2021). Properties of binary complexes of whey protein fibril and gum Arabic and their functions of stabilizing emulsions and simulating mayonnaise. *Innovative Food Science & Emerging Technologies, 68*, Article 102609.

Tang, C. (2020). Globular proteins as soft particles for stabilizing emulsions: Concepts and strategies. *Food Hydrocolloids, 103*, Article 105664.

Verkade, P. (2012). Electron microscopy (TEM and SEM). *Essential Guide to Reading Biomedical Papers: Recognising and Interpreting Best Practice*, 59–65.

Visser, D., Loo, T., Norris, G., & Parry, D. A. (2023). Potential implications of the glycosylation patterns in collagen α1 (I) and α2 (I) chains for fibril assembly and growth. *Journal of Structural Biology, 215*(1), Article 107938.

Vogelsang-O'Dwyer, M., Petersen, I. L., Joehnke, M. S., Sørensen, J. C., Bez, J., Detzel, A., et al. (2020). Comparison of Faba bean protein ingredients produced using dry fractionation and isoelectric precipitation: Techno-functional, nutritional and environmental performance. *Foods, 9*(3), 322.

Wang, Y., Shen, Y., Qi, G., Li, Y., Sun, X. S., Qiu, D., et al. (2020). Formation and physicochemical properties of amyloid fibrils from soy protein. *International Journal of Biological Macromolecules, 149*, 609–616.

Wang, S., Xie, Y., Ding, Y., Huo, Z., Li, J., Song, J., et al. (2023). Fibrillation of whey protein isolate by radio frequency heating for process efficiency: Assembly behavior, structural characteristics, and in-vitro digestion. *Innovative Food Science & Emerging Technologies, 88*, Article 103436.

Wei, Z., Cheng, J., & Huang, Q. (2019). Food-grade Pickering emulsions stabilized by ovotransferrin fibrils. *Food Hydrocolloids, 94*, 592–602.

Wei, Z., & Huang, Q. (2020). Impact of covalent or non-covalent bound epigallocatechin-3-gallate (EGCG) on assembly, physicochemical characteristics and digestion of ovotransferrin fibrils. *Food Hydrocolloids, 98*, Article 105314.

Wen, C., Zhang, J., Yao, H., Zhou, J., Duan, Y., Zhang, H., et al. (2019). Advances in renewable plant-derived protein source: The structure, physicochemical properties affected by ultrasonication. *Ultrasonics Sonochemistry, 53*, 83–98.

Wood, K., Mata, J. P., Garvey, C. J., Wu, C.-M., Hamilton, W. A., Abbeywick, P., et al. (2018). QUOKKA, the pinhole small-angle neutron scattering instrument at the OPAL research reactor, Australia: Design, performance, operation and scientific highlights. *Journal of Applied Crystallography, 51*(2), 294–314.

Wu, H., Nian, Y., Liu, Y., Zhang, Y., & Hu, B. (2022). Formation of pea protein amyloid fibrils to stabilize high internal phase emulsions for encapsulation of lutein. *Journal of Functional Foods, 94*, Article 105110.

Wynnychuk, C., Jo, Y.-J., Chu, Y., & Chen, L. (2021). Long-term stable emulsions prepared from lentil protein fibrillar aggregates. *Food Structure, 29*, Article 100204.

Xu, Y., Ma, C.-m., Yang, Y., Bian, X., Liu, X.-f., Wang, Y., et al. (2023a). Food-derived protein amyloid-like fibrils: Fibrillation mechanism, structure, and recent advances for the stabilization of emulsions. *Food Hydrocolloids*, Article 109146.

Xu, Z., Shan, G., Hao, N., Li, L., Lan, T., Dong, Y., et al. (2022). Structure remodeling of soy protein-derived amyloid fibrils mediated by epigallocatechin-3-gallate. *Biomaterials, 283*, Article 121455.

Xu, Z., Wang, X., Gao, Y., Zhang, Y., Jiang, L., & Sui, X. (2023b). Structural insights into acidic heating-induced amyloid fibrils derived from soy protein as a function of protein concentration. *Food Hydrocolloids, 145*, Article 109085.

Yagi, H., Hasegawa, K., Yoshimura, Y., & Goto, Y. (2013). Acceleration of the depolymerization of amyloid β fibrils by ultrasonication. *Biochimica et Biophysica Acta (BBA) - Proteins & Proteomics, 1834*(12), 2480–2485.

Yang, Z., de Campo, L., Gilbert, E. P., Knott, R., Cheng, L., Storer, B., et al. (2022a). Effect of NaCl and $CaCl_2$ concentration on the rheological and structural characteristics of thermally-induced quinoa protein gels. *Food Hydrocolloids, 124*, Article 107350.

Yang, Z., Hemar, Y., Hilliou, L., Gilbert, E. P., McGillivray, D. J., Williams, M. A., et al. (2016). Nonlinear behavior of gelatin networks reveals a hierarchical structure. *Biomacromolecules, 17*(2), 590–600.

Yang, Y., Jiao, Q., Wang, L., Zhang, Y., Jiang, B., Li, D., et al. (2022b). Preparation and evaluation of a novel high internal phase Pickering emulsion based on whey protein isolate nanofibrils derived by hydrothermal method. *Food Hydrocolloids, 123*, Article 107180.

Yang, Z., Yang, H., & Yang, H. (2018). Effects of sucrose addition on the rheology and microstructure of κ-carrageenan gel. *Food Hydrocolloids, 75*, 164–173.

Ye, X., Lendel, C., Langton, M., Olsson, R. T., & Hedenqvist, M. S. (2019). Protein nanofibrils: Preparation, properties, and possible applications in industrial nanomaterials. In *Industrial applications of nanomaterials* (pp. 29–63). Elsevier.

Yi, J., He, Q., Peng, G., & Fan, Y. (2022). Improved water solubility, chemical stability, antioxidant and anticancer activity of resveratrol via nanoencapsulation with pea protein nanofibrils. *Food Chemistry, 377*, Article 131942.

Yu, Z., Li, N., Liu, Y., Zhang, B., Zhang, M., Wang, X., et al. (2024). Formation, structure and functional characteristics of amyloid fibrils formed based on soy protein isolates. *International Journal of Biological Macromolecules, 254*, Article 127956.

Zhang, R., Cheng, L., Luo, L., Hemar, Y., & Yang, Z. (2021a). Formation and characterisation of high-internal-phase emulsions stabilised by high-pressure homogenised quinoa protein isolate. *Colloids and Surfaces A: Physicochemical and Engineering Aspects, 631*, Article 127688.

Zhang, Y., & Dee, D. R. (2023). Morphology, formation kinetics and core composition of pea and soy 7S and 11S globulin amyloid fibrils. *Journal of Agricultural and Food Chemistry, 71*(11), 4755–4765.

Zhang, Y.-H., & Huang, L.-H. (2014). Effect of heat-induced formation of rice bran protein fibrils on morphological structure and physicochemical properties in solutions and gels. *Food Science and Biotechnology, 23*, 1417–1423.

Zhang, Y., Liang, S., Zhang, J., Chi, Y., Tian, B., Li, L., et al. (2020). Preparation of whey protein isolate nanofibrils by microwave heating and its application as carriers of lipophilic bioactive substances. *Lebensmittel-Wissenschaft & Technologie, 125*, Article 109213.

Zhang, F., Roosen-Runge, F., Skoda, M. W., Jacobs, R. M., Wolf, M., Callow, P., et al. (2012). Hydration and interactions in protein solutions containing concentrated electrolytes studied by small-angle scattering. *Physical Chemistry Chemical Physics, 14*(7), 2483–2493.

Zhang, X., Zuo, Z., Ma, W., Yu, P., Li, T., & Wang, L. (2021b). Assemble behavior of ultrasound-induced quinoa protein nanoparticles and their roles on rheological properties and stability of high internal phase emulsions. *Food Hydrocolloids, 117*, Article 106748.

Zhong, Z., & Xiong, Y. L. (2020). Thermosonication-induced structural changes and solution properties of mung bean protein. *Ultrasonics Sonochemistry, 62*, Article 104908.

Zhou, J., Li, T., Peydayesh, M., Usuelli, M., Lutz-Bueno, V., Teng, J., et al. (2022). Oat plant amyloids for sustainable functional materials. *Advanced Science, 9*(4), Article 2104445.

Zhou, Q., Lv, S., Wang, W., Zhu, S., Xu, J., Zheng, M., et al. (2024). Remodeling mechanism of gel network structure of soy protein isolate amyloid fibrils mediated by cellulose nanocrystals. *Carbohydrate Polymers*, Article 121919.

Zhu, P., Huang, W., & Chen, L. (2022). Develop and characterize thermally reversible transparent gels from pea protein isolate and study the gel formation mechanisms. *Food Hydrocolloids, 125*, Article 107373.